High-temperature geochronology constraints on the tectonic history and architecture of the ultrahigh-pressure Dabie-Sulu Orogen

Bradley R. Hacker,[1] Simon R. Wallis,[2] Lothar Ratschbacher,[3] Marty Grove,[4] and George Gehrels[5]

Received 16 December 2005; revised 25 May 2006; accepted 15 August 2006; published 20 October 2006.

[1] New U/Pb zircon and Th/Pb monazite ages are presented from the giant Sulu ultrahigh-pressure (UHP) terrane. Combined with Sm/Nd ages, Rb/Sr ages, inclusion relationships, and geologic relationships, they help define the timing of peak recrystallization, the timing of subsequent amphibolite-facies metamorphism, and the architecture of the Dabie-Sulu suture zone between the collided Sino-Korean and Yangtze cratons. The data indicate a ~15 Myr record of UHP recrystallization, the first clearly documented for a giant UHP terrane; this requires that continental subduction in the Dabie-Sulu orogen involved multiple UHP tectonic or recrystallization events. A 244–236 Ma "precursor" UHP event, seen only in the Dabie Shan, was followed by a second, ~230–220 Ma "main" UHP event, which was itself terminated by a 220–205 Ma amphibolite-facies overprint. Older eclogite-facies events seen in the Qinling segment of this orogenic belt raise the possibility that these rocks have undergone (U)HP metamorphism three or four times, but at present, there is no geochronological evidence in the Dabie-Sulu area to support this. The subduction of the lower, Yangtze plate did not proceed in a simple fashion: The ages of inherited zircon cores demonstrate that a ribbon continent of Yangtze affinity escaped subduction and became wedged against the Sino-Korean plate hanging wall. **Citation:** Hacker, B. R., S. R. Wallis, L. Ratschbacher, M. Grove, and G. Gehrels (2006), High-temperature geochronology constraints on the tectonic history and architecture of the ultrahigh-pressure Dabie-Sulu Orogen, *Tectonics*, *25*, TC5006, doi:10.1029/2005TC001937.

1. Introduction

[2] Ultrahigh-pressure (UHP) terranes are defined by the presence of regionally developed metamorphic coesite and are composed of crustal rocks that were subducted to and exhumed from mantle depths >100 km. The Qinling-Dabie-Sulu orogen of China contains one of Earth's three giant UHP terranes. Several features render this UHP orogen one of the best for understanding the generation and exhumation of UHP rocks: (1) UHP rocks cover an area exceeding 10,000 km^2; (2) the presence of carbonates, phosphates, basalts, and quartzites proves that the UHP rocks represent in part a subducted supracrustal sequence [*Rolfo et al.*, 2004] and are not simply overthickened lower crust; and (3) well-documented peak metamorphism of 650–850°C and 4 GPa [*Hacker et al.*, 1997; *Zhang and Liou*, 1998; *Mattinson et al.*, 2004; *Proyer et al.*, 2004] shows that this terrane was subducted to and exhumed from depths of 135 km.

[3] Central to resolving the physical and chemical processes involved in the genesis and exhumation of UHP terranes is constraining the sequence of events. Simple questions like the following remain poorly answered: "How rapid was continental subduction?" "How many UHP event(s) were there?" "How long did the UHP event(s) last?" In the specific case of the giant Qinling-Dabie-Sulu UHP terrane, we know that it developed during northward subduction of the Yangtze Craton beneath the Sino-Korean Craton in the Triassic [*Hacker et al.*, 2000], but important controversies include the following: Exactly when in the Triassic did the UHPM occur? Were UHP subduction and exhumation coeval everywhere along the length of the orogen, implying a short-lived subduction and exhumation event of regional extent, or were they diachronous? Are some of the eclogites assumed to be Triassic actually remnants of early (U)HP metamorphic events? Where is the suture between the upper and lower plates in the collision zone? This paper addresses these issues with new U/Pb zircon and monazite ages from the Sulu area, introduced below. We present both multicollector inductively coupled plasma mass spectrometry (ICP) and secondary ion mass spec-

[1]Department of Geological Sciences, University of California, Santa Barbara, California, USA.
[2]Department of Earth and Planetary Sciences, Graduate School of Environmental Studies, Nagoya University, Nagoya, Japan.
[3]Institut für Geowissenschaften, Technische Universität Bergakademie Freiberg, Freiberg/Sachsen, Germany.
[4]Department of Earth and Space Sciences, University of California, Los Angeles, California, USA.
[5]Department of Geosciences, University of Arizona, Tucson, Arizona, USA.

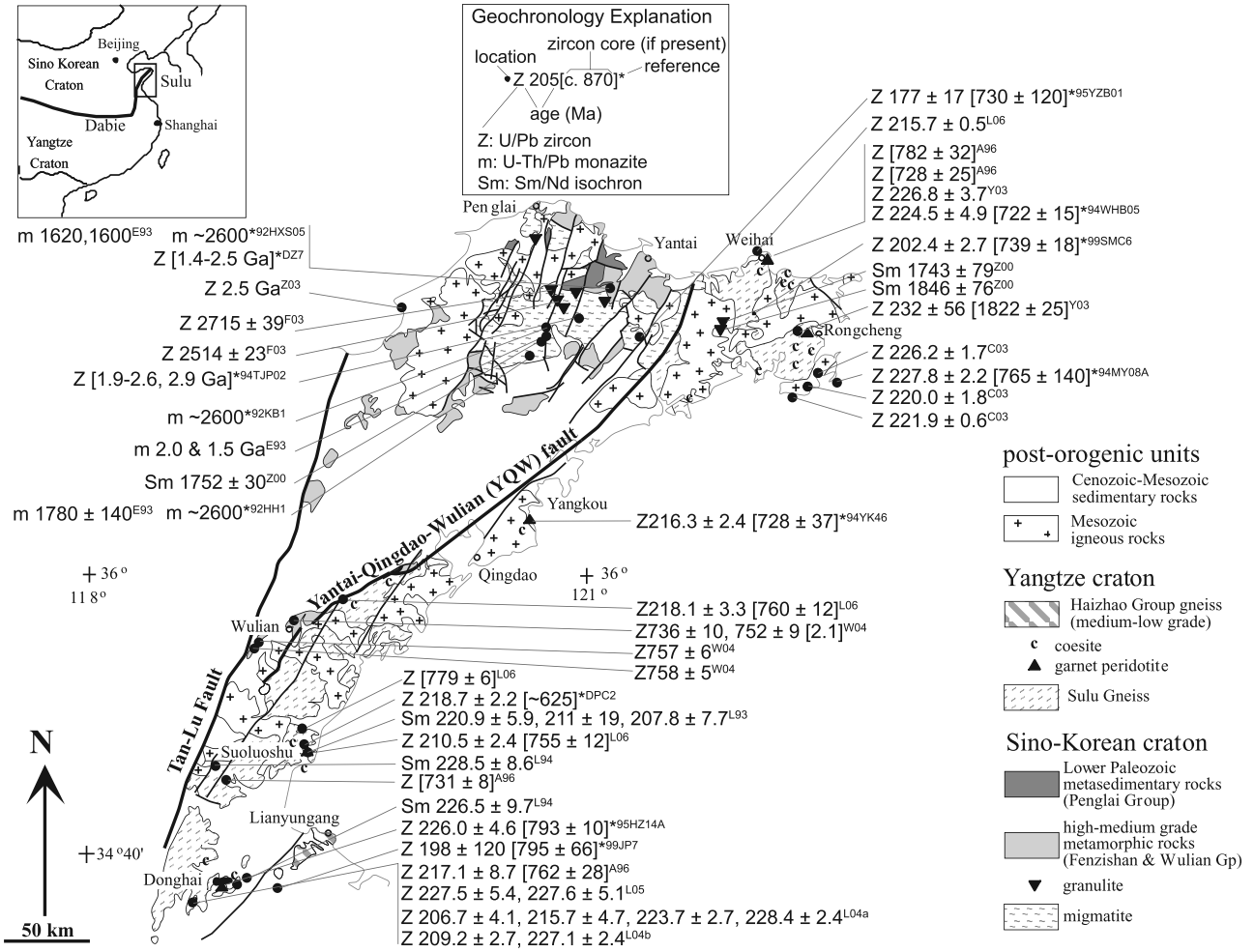

Figure 1. Geology of the Shandong area [after *Regional Geological Survey of Jiangsu*, 1984; *Regional Geological Survey of Shandong*, 1991; *Faure et al.*, 2003; *Wu et al.*, 2004], emphasizing high-temperature geochronology. Coesite and coesite pseudomorphs locales from *Zhang and Liou* [1998]. High-pressure granulite blocks from *Zhai et al.* [2000] and *Faure et al.* [2003]. References: asterisk, this study; A96 [*Ames et al.*, 1996]; C03 [*Chen et al.*, 2003b]; E93 [*Enami et al.*, 1993]; F03 [*Faure et al.*, 2003]; L93 [*Li et al.*, 1993]; L94 [*Li et al.*, 1994]; L04a [*Liu et al.*, 2004a]; L04b [*Liu et al.*, 2004b]; L05 [*Liu et al.*, 2005]; L06 [*Leech et al.*, 2006]; W04 [*Wu et al.*, 2004]; Y03 [*Yang et al.*, 2003b]; Z00 [*Zhai et al.*, 2000]; Z03 [*Zhou et al.*, 2003].

trometry (SIMS) ages and compare them with an isotopically and regionally broader data set.

2. Geology of Sulu

[4] The Shandong peninsula in eastern China contains one of the great HP and UHP regions on Earth (Figure 1). It is separated into two domains separated by the Yantai-Qingdao-Wulian (YQW) fault system. Northwest of this fault the basement rocks are banded mafic to felsic gneisses. These gneisses are dominantly amphibolite facies but locally preserve granulite-facies relics [*Zhai et al.*, 2000]; no eclogite is known. Ultramafic rocks are rare and exclusively spinel peridotite. The basement gneisses are overlain by a series of medium-grade to unmetamorphosed rocks of Archean(?), Proterozoic, and lower Paleozoic age known as the Jiaodong, Fenzishan, Jingshan-Wulian, and Penglai groups [*Wu et al.*, 2004]. Differentiating among these groups is difficult, but the Wulian and Penglai groups have Sinian fossils [*Zhou et al.*, 1995], generally low-grade metamorphism, and the same heterogeneous rock types (see below), even though they are exposed in different regions (Wulian in the southwestern and Penglai in the northeastern Shandong peninsula).

[5] Southeast of the YQW fault the basement rocks (“Sulu gneiss”) are dominantly banded felsic gneisses containing ultramafic and mafic blocks with local coesite-eclogite parageneses. In some regions the felsic gneisses preserve features characteristic of granites [*Wallis et al.*, 1997] and in other regions are intercalated with lenses of dolomitic marble and schist [*Kato et al.*, 1997], but no clear evidence proves a metasedimentary or meta-igneous origin

for all the gneisses. The UHP and HP eclogites and garnet peridotites reached conditions of 650–850°C and 4 GPa; this UHP metamorphism was followed by a strong amphibolite- to granulite-facies overprint at 750°C and 1 GPa that nearly erased the record of the UHP event [*Zhang et al.*, 1995; *Banno et al.*, 2000; *Nakamura and Hirajima*, 2000]. Rocks on both sides of the YQW fault are intruded by numerous granitoid bodies of chiefly Jurassic to Cretaceous age [*Yang et al.*, 2005b] and unconformably overlain by dominantly volcaniclastic Mesozoic to Cenozoic sediments.

[6] Traditionally the metamorphic differences across the YQW fault, in particular the absence of eclogite to the northwest, have been taken as evidence that the Yangtze Craton and the Sulu UHP-HP terrane are restricted to the southeast side of the fault and that the Sino-Korean Craton is restricted to the northwest side. However, the basement rocks on both sides of the YQW fault have a strong amphibolite-facies overprint that largely obscures earlier metamorphic assemblages, and both sides contain local granulite-facies rocks [*Banno et al.*, 2000; *Nakamura and Hirajima*, 2000]. *Faure et al* [2001, 2003] used this similarity to challenge the traditional interpretation, suggesting that some of the amphibolite-facies rocks northwest of the YQW fault are retrogressed eclogite. They used their new interpretation to suggest that the suture lies west of the YQW fault and that the entire Shandong peninsula is a regional sheet of low- to medium-grade metamorphic rocks overlying UHP/HP rocks. If correct, this constitutes a major reinterpretation and requires revision of all tectonic models explaining the formation and exhumation of the Sulu UHP rocks. We agree in this paper that rocks northwest of the YQW are of Yangtze craton affinity, but we suggest instead that they belong to the Qinling microcontinent [*Ratschbacher et al.*, 2003, 2004] that was rifted from the Yangtze craton in the Proterozoic and thereby escaped the Triassic UHP metamorphism.

3. New Geochronology

[7] We measured U-Pb and Th-Pb ages from Sulu zircons and monazites to understand the orogen architecture and the causal events, taking care to study rocks giving extensive areal coverage of both sides of the YQW fault and localities that have played an important role in revealing the UHP petrological history (see Figure 1 and the auxiliary material for analytical methods).[1] We chose to focus on the quartz-feldspathic gneisses that host the eclogites because they are volumetrically dominant and have seen limited U/Pb study; undeformed or weakly deformed igneous rocks were not dated.

[8] Sample 94TJP02 is a strongly foliated biotite-granite gneiss with well-developed compositional layering from north of the YQW fault. This sample was examined to evaluate whether the effects of the UHP reached this far north. Abundant, pink-yellow-colorless zircons show cathodoluminescent (CL) oscillatory zoning to higher U rims, but little resorbtion and no sector zoning, suggestive of igneous crystallization (Figure 2). Although differences in precision exist between the SIMS and ICP data (Figures 3–5), the combined results indicate (re)crystallization between 2.9 and 2.5 Ga and subsequent (re)crystallization around 1.9–1.8 Ga. The CL textures and Th/U ratios of 0.1–0.6 imply that both crystallization events are magmatic [cf. *Hoskin and Schaltegger*, 2003].

[9] DZ7 is an orthogneiss with quenched melt intruded along decimeter- to centimeter-scale shear zones. This sample is also from north of the YQW fault. The presence of clear partial melting zones associated with deformation [see *Wallis et al.*, 1999, Figures 5a and 5b] suggests dating of these samples may allow determination of melting and its associated tectonic event. Zircons extracted from the former melt have cathodoluminescent, partly oscillatory cores overgrown by dark mottled rims (Figure 2). A discordia defined by combined ICP + SIMS results indicates initial (re)crystallization at ~2.5 Ga followed by (re)crystallization around 1.4 Ga (Figure 3b). The ICP results derive from relatively large zircon volumes whereas the SIMS results targeted only the thin overgrowths present on some of the zircons. If the ICP analyses alone are used to constrain the upper intercept, a concordia age (in the sense of *Ludwig* [1998]) of 2486 ± 36 Ma is obtained (Figure 3b inset). Forcing the upper intercept to 2486 ± 36 Ma and projecting through the SIMS data gives a lower intercept of 1418 ± 62 Ma. Th/U ratios of ~0.6 suggest that these events were igneous.

[10] The sample 95YZB01 is a strongly deformed granitic orthogneiss located immediately northwest of the YQW fault. It lacks the clear compositional layering of the previous two samples. It contains sparse pale brown to pale red zircons for which CL images show oscillatory zoned grains with no obvious rims (Figure 2). Relatively high Th/U ratios of ~0.8 suggest that these grains are igneous. ICP $^{206}Pb/^{238}U$ spot ages on 11 grains range from 149 to 713 Ma. A discordia fit to all the data yields an upper intercept of 730 ± 120 Ma and a lower intercept of 177 ± 17 Ma (Figure 3c). The younger spot ages form a single subpopulation with a concordia age of 160.4 ± 2.3 Ma (inset). We interpret this as the crystallization age of the granite; the strong fabric of this rock implies that tectonism continued through the Late Jurassic in this area.

[11] The sample 94MY08A is a compositionally layered granitic orthogneiss from the northern part of the UHP domain. It contains large K-feldspar grains up to 20 cm in size [see *Wallis et al.*, 1999, Figure 5e]. A first, folded foliation is truncated by a second foliation, implying a complex tectonic history and hinting at an origin older than the less deformed Jurassic granite sample 95YZB01. The zircon grains show patchy or mottled CL (Figure 2). The oldest spot from a high Th/U core has a concordant $^{206}Pb/^{238}U$ age of 862 Ma. A discordia fit to all the data yields intercepts of 765 ± 135 Ma and 230 ± 13 Ma (Figure 3d) confirming a Precambrian origin for this gneiss. Most of the $^{206}Pb/^{238}U$ spot ages are younger than ~270 Ma (Figure 4a) and have Th/U ratios of 0.01–0.06, suggesting that they are metamorphic. Twenty of these ages (excepting only the youngest,

[1] Auxiliary material data sets are available at ftp://ftp.agu.org/apend/tc/2005tc001937. Other auxiliary material files are in the HTML.

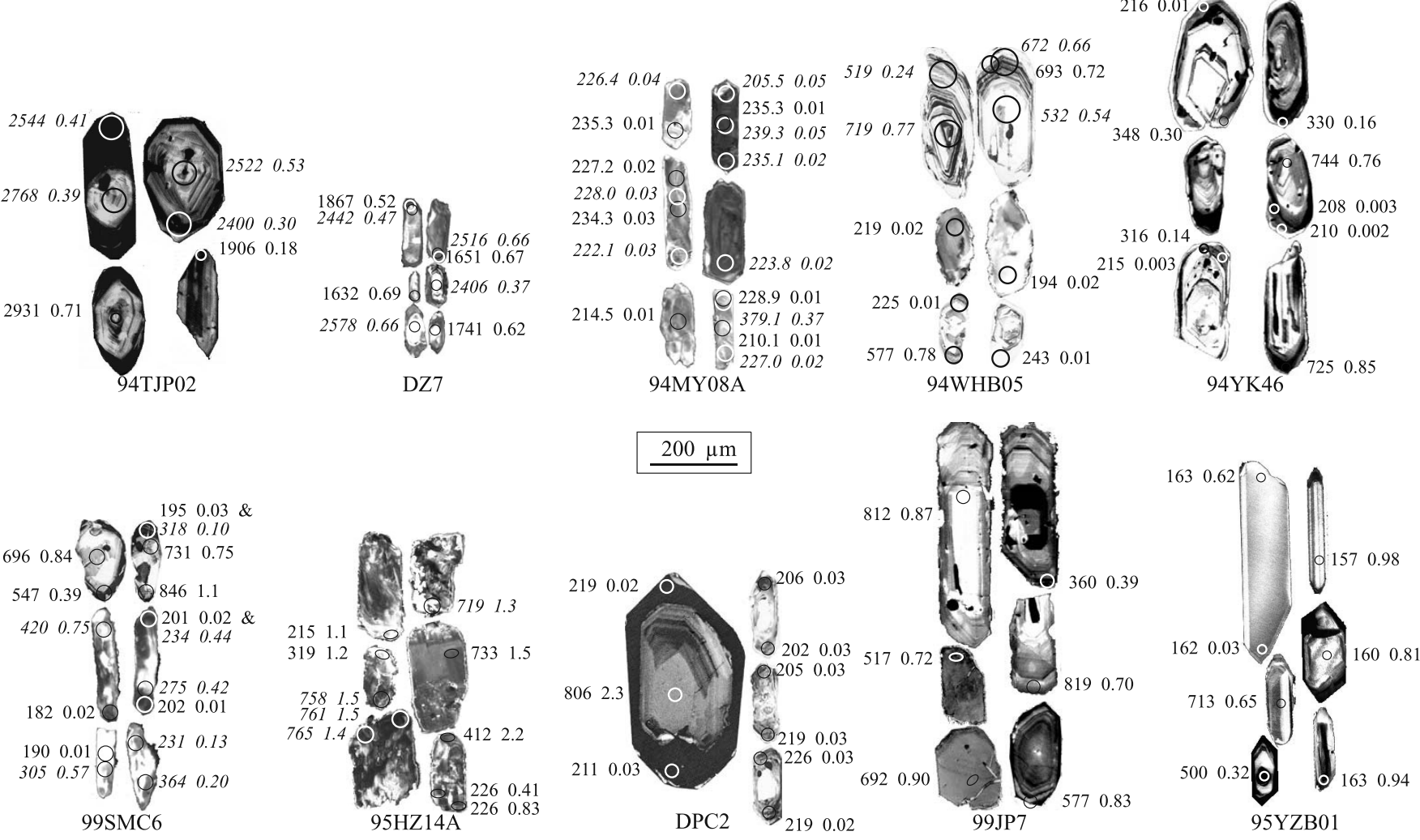

Figure 2. Cathodoluminescence images of typical zircons. SIMS data are shown in normal text, and ICP data are italicized. First number is age in Ma, and second number is Th/U ratio.

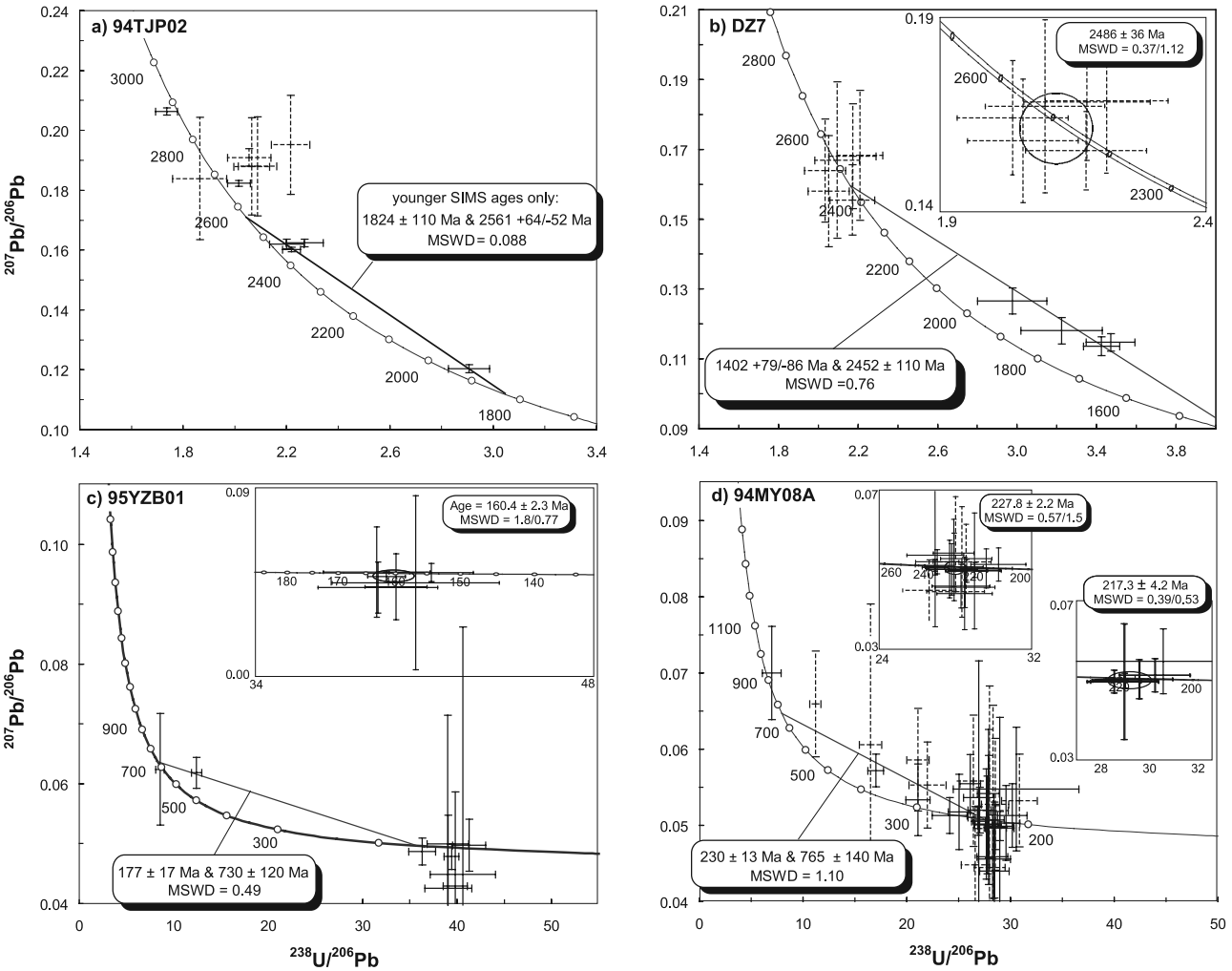

Figure 3. Tera-Wasserburg presentations of U/Pb isotopic data corrected using measured ^{204}Pb. ICP data are dashed; SIMS data are solid lines. Error crosses are 2σ. Where two MSWDs are given for concordia ages, they correspond to the ''concordance'' and ''concordance plus equivalence'' tests of Isoplot.

206 Ma) from ICP and SIMS analyses define a single population with a concordia age of 227.8 ± 2.2 Ma (Figure 3d). The youngest group of five SIMS ages yields a slightly younger concordia age of 217.3 ± 4.2 Ma; these analyses do not show distinctly different U contents, Th/U ratios, or CL response compared to the ICP analyses, and may give younger ages simply because SIMS consumes ~2 orders of magnitude less zircon and is therefore more likely to capture the effects of small amounts of Pb loss. Because these five SIMS analyses were obtained from the near-rim regions, we interpret these results as reflecting Pb loss subsequent to the recrystallization age yielded by the bulk of the zircon and the ICP analyses. For this reason, we use the concordia age for the remaining 15 spots of 229.5 ± 5.6 Ma (mean square weighted deviation (MSWD) = 0.52) as the best peak metamorphic age for this sample.

[12] The sample 94WHB05 is a strongly deformed, compositionally layered biotite–K-feldspar augen gneiss from Weihai in the northern part of the UHP domain. This region shows local evidence for partial melting [*Wallis et al.*, 1999, Figure 5c]. The zircons show oscillatory-zoned cores with mottled CL rims (Figure 2). Thirty-one ^{206}Pb/^{238}U ICP spot ages on 16 grains range from 171 to 792 Ma. A discordia fit to all the data yields intercepts of 670 ± 52 Ma and 225 ± 22 Ma (Figure 5a). Five of the oldest spot ages from grain cores yield a concordia age of 722 ± 15 Ma. Three of these youngest points give a concordia age of 224.5 ± 4.9 Ma and the two most precise ages have a weighted mean ^{206}Pb/^{238}U age of 223.7 ± 4.9 Ma (Figure 4b). Although the geologic significance of ages calculated from these low Th/U (0.01–0.02) spots is difficult to assess given the meager number of Mesozoic spot ages, continued Pb loss into the Late Triassic is indicated. Both Cretaceous and Triassic ages have been reported from this region [*Wallis et al.*, 1999].

[13] The sample 94YK46 is a phengite-K-feldspar granitic gneiss from Yangkou in the northern part of the UHP domain showing weak compositional layering. The

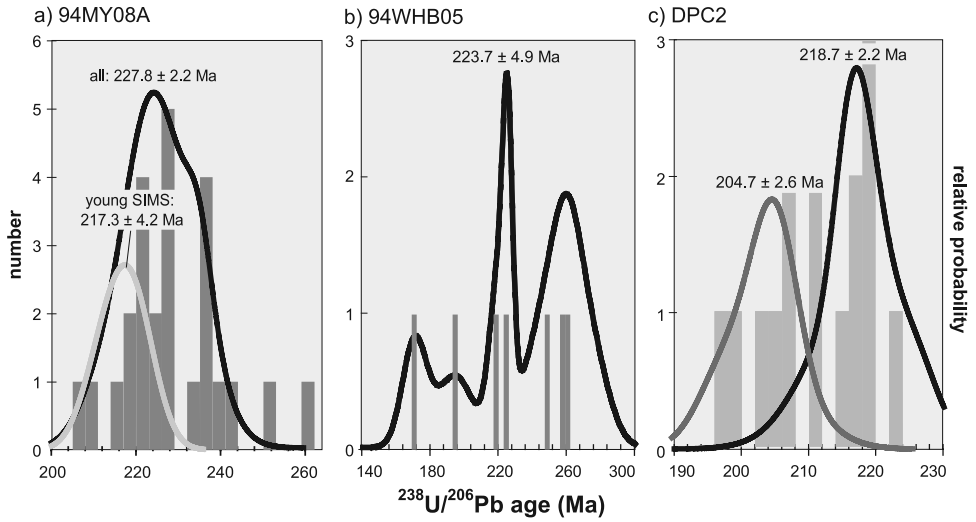

Figure 4. Histograms and relative frequencies of young $^{238}U/^{206}Pb$ ages from three samples. The older and younger ages for 94MY08A and DPC2 are interpreted to reflect peak metamorphism and Pb loss, respectively.

Yangkou area is best known for studies of the Yangkou unit [*Wallis et al.*, 1997] that preserves coesite as a matrix mineral, implying low fluid activity during and after UHP metamorphism [*Liou and Zhang*, 1996]. Probably as a result of this low fluid activity, zircon shows very little evidence for new growth associated with the UHP metamorphism [*Wallis et al.*, 2005]. The sample used in the present study comes from outside the Yangkou unit and is more likely to have undergone zircon growth related to the UHP metamorphism. The zircons are abundant, pale yellow to orange to colorless, inclusion-free grains. CL images show oscillatory-zoned cores overgrown by thin rims with relatively flat CL response (Figure 2). Twenty ICP $^{206}Pb/^{238}U$ spot ages on 17 grains range from 188 to 744 Ma. A discordia fit to all the data yields intercepts of 728 ± 37 Ma and 226 ± 14 Ma (Figure 5b). The six youngest, low Th/U grains give a concordia age of 216.3 ± 2.4 Ma. All grains older than 223 Ma show a positive linear correlation between Th/U and $^{206}Pb/^{238}U$ spot age, whereas all six younger grains have a fixed Th/U ratio of 0.013 (Figure 6a); there is no correlation between age and U content, which is low, at 100–500 ppm. It is probable therefore that the U-Pb ages older than 223 Ma are from analyses of domains with mixed <223 Ma and ~750 Ma zircon.

[14] The sample 99SMC6 is a biotite–K-feldspar gneiss with compositional layering showing two stages of deformation from close to Rongcheng in the northern part of the UHP domain. This gneiss locally contains garnet and textural evidence for partial melting and is cut by small undeformed dikes. CL images show mottled overgrowths on cores with oscillatory zoning (Figure 2). Thirty-one ICP $^{206}Pb/^{238}U$ spot ages on 26 grains range from 182 to 846 Ma. Like sample 94YK46, there is a positive correlation between Th/U and age for grains older than 206 Ma and a fixed Th/U ratio of ≤0.02 for younger grains (Figure 6b). In similar fashion to 94YK46, this implies that most $^{206}Pb/^{238}U$ spot ages are mixtures of ~206 Ma and ~750 Ma zircon age domains. A discordia fit to all the data yields intercepts of 868 ± 150 Ma and 229 ± 35 Ma (Figure 5c). The four oldest spot ages from grain cores yield a concordia age of ~739 ± 18 Ma. Of the eight spot ages with low Th/U, the oldest six have a concordia age of 202.4 ± 2.7 Ma; their high U contents of 1700–2900 ppm suggest that they are affected by Pb loss.

[15] The sample 95HZ14A is a mica–K-feldspar deformed granite from Donghai in the southern part of the UHP domain. There is very little evidence for either partial melting or late stage igneous intrusion in this region. It is, however, unclear whether these deformed granites can be correlated with the compositionally layered gneiss in the northern part of the UHP region. The sample contains orange, partly rounded zircons, with oscillatory-zoned cores overgrown by <10 μm thick rims with variable and mottled CL response (Figure 2). Twenty-nine ICP $^{206}Pb/^{238}U$ spot ages on 25 grains range from 214 to 814 Ma. A discordia fit to all the data yields intercepts of 768 ± 14 Ma and ~206 ± 23 Ma (Figure 5d). Three of the oldest spot ages from grain cores have a concordia age of 793.4 ± 10 Ma. The three youngest low Th/U spots yield a concordia age of 221.8 ± 7.3 Ma. Two points have a concordia age of 226.0 ± 4.6 Ma, in closer agreement with the better constrained results from samples 94MY08A and 94WHB05. These results show that the original pre-UHP basement complex contained local granite bodies.

[16] DPC2 is a granitic orthogneiss with well-defined compositional layering from Suoluoshu in the southern part of the UHP domain. At least two phases of folding are preserved. Local centimeter-scale garnet clusters and aegerine are found in the gneiss. CL images of the zircons show mottled, diffusely luminescent rims on cores with oscillatory zoning (Figure 2). There is a sharp discontinuity in Th/U ratios from ~1 in the cores to <0.03 in the rims.

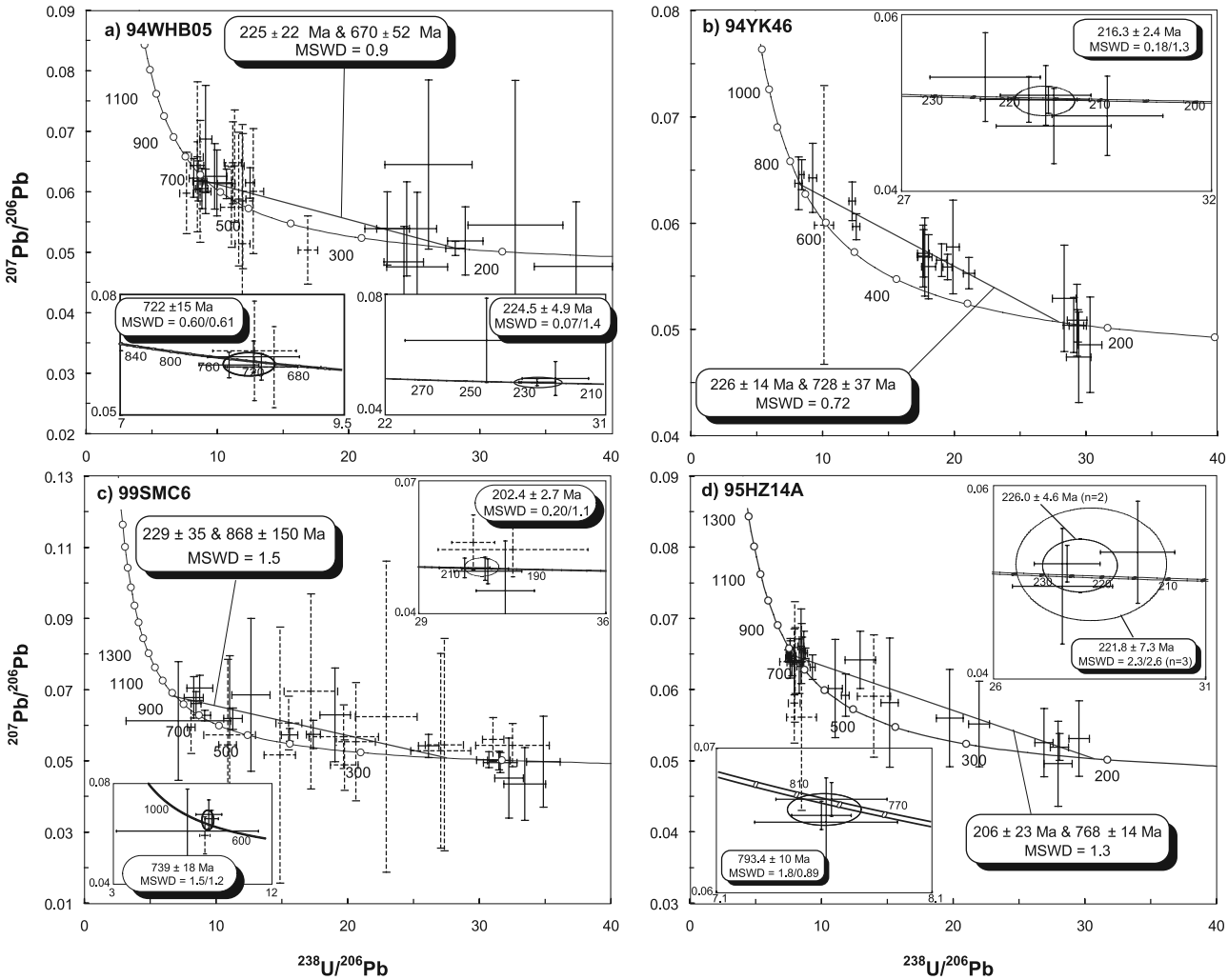

Figure 5. Tera-Wasserburg presentations of U/Pb isotopic data corrected using measured ^{204}Pb. ICP data are dashed; SIMS data are solid lines. Error crosses are 2σ. Where two MSWDs are given for concordia ages, they correspond to the concordance and concordance plus equivalence tests of Isoplot.

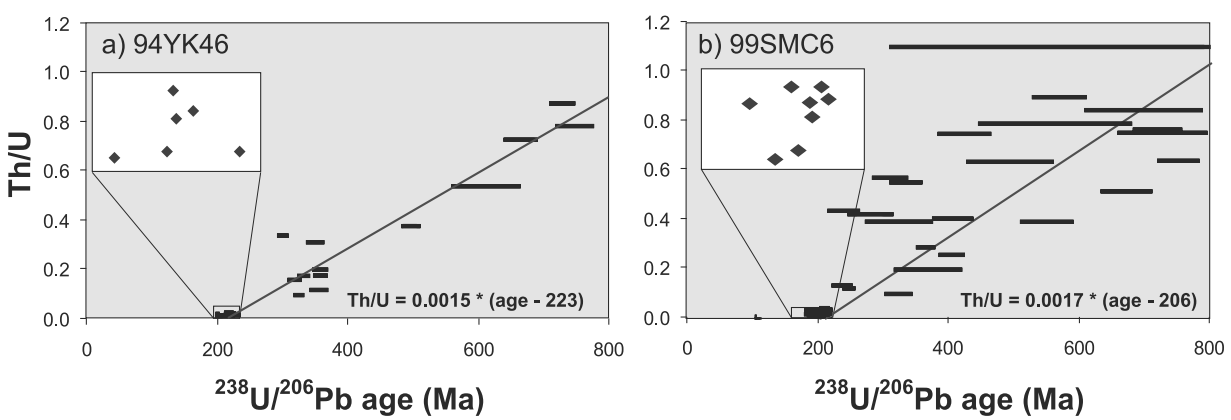

Figure 6. Clear correlation between Th/U and ^{238}U/^{206}Pb age in samples 94YK46 and 99SMC6 suggesting analysis of overlapping age domains.

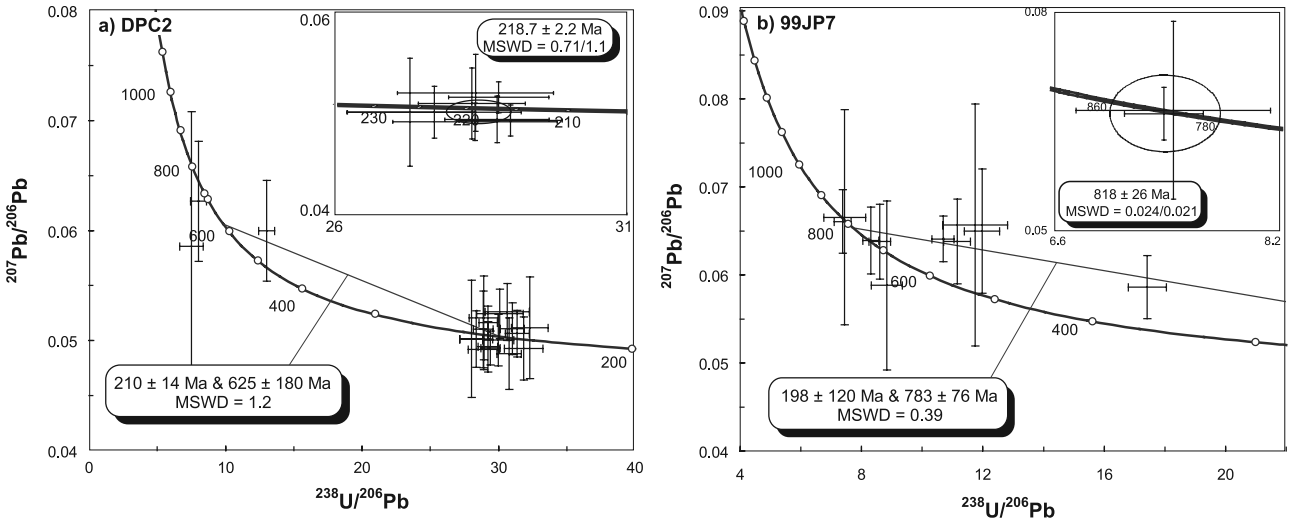

Figure 7. Tera-Wasserburg presentations of U/Pb isotopic data corrected using measured ^{204}Pb. ICP data are dashed; SIMS data are solid lines. Error crosses are 2σ. Where two MSWDs are given for concordia ages, they correspond to the concordance and concordance plus equivalence tests of Isoplot.

Nineteen ICP $^{238}U/^{206}Pb$ spot ages on 16 grains range from 197 to 806 Ma. A discordia fit to all the spot ages gives intercepts of 625 ± 180 Ma and 210 ± 14 Ma (Figure 7a). The two oldest spot ages from grain cores yield a concordia age of 764 ± 43 Ma. The $^{206}Pb/^{238}U$ ages from the low Th/U analyses show two subpopulations, each defined by eight analyses (Figure 4c). The two groups have concordia ages of 218.7 ± 2.2 Ma and 204.7 ± 2.6 Ma, and show no differences in U content.

[17] The sample 99JP7 is a quartzfeldspathic schist likely derived from a granite near Lianyungang. Field observations suggest this schist overlies the main gneiss region, probably along an unconformable contact. It has abundant, frosted, inclusion-rich, whitish opaque to clear zircons. CL images show oscillatory-zoned, mottled grains with no evident rims (Figure 2). Most of the ICP analyses yield relatively high Th/U ratios of ~0.6, suggesting that these grains are igneous; one grain has a slightly lower Th/U rim. The two oldest spot ages from grain cores yield a concordia age of 818 ± 26 Ma. A discordia fit to all the data yields intercepts of 783 ± 76 Ma and 198 ± 120 Ma (Figure 7b). These data indicate igneous crystallization at ~818 Ma and probable Jura-Triassic Pb loss. These results suggest the sedimentary cover to the Sulu gneiss was also involved in the Triassic orogeny and metamorphism.

[18] *Enami et al.* [1993] described in detail four monazite-bearing sillimanite–K-feldspar–garnet–biotite schists from SW of Yantai that they dated using an electron microprobe. We dated monazite from three similar schists, 92HH1, 92HXS05, and 92KB1, from the same area. The monazites are commonly intergrown with and locally completely included by grains of aligned biotite; texturally distinct cores are observed in some grains. A broad range in monazite Th/Pb ages from 2068 Ma to 347 Ma (Figure 8) suggests, at the minimum, a post-347 Ma overprint of a pre-2068 Ma metamorphism. As a means of unraveling the timing of the UHP and subsequent amphibolite-facies events, however, the monazite ages are not helpful, and not discussed further.

4. Discussion

[19] Our new data and the entire Sm/Nd, U/Pb, Th/Pb, and Rb/Sr data set from the Sulu-Dabie area can be combined to address the questions posed in the introduction: the timing of UHP and overprinting events, including assessing whether there were multiple UHP events, whether the UHP metamorphism might have been diachronous, and the location of the suture between the colliding plates.

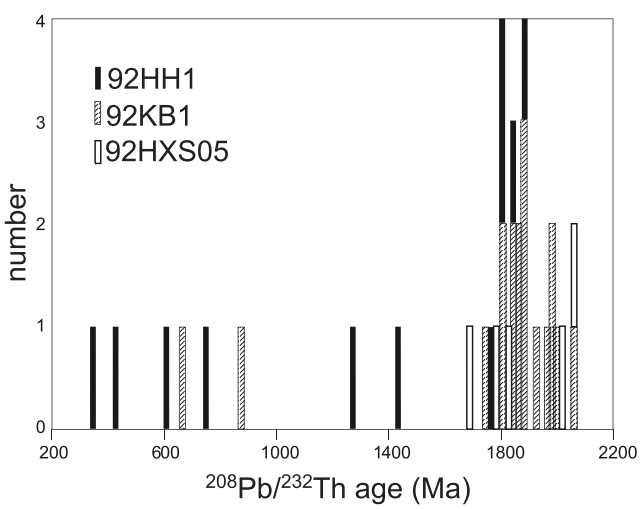

Figure 8. The $^{232}Th/^{208}Pb$ ages for monazites 92HH1, 92HXS05, and 92KB01.

4.1. Interpretation of the New U/Pb Zircon Ages From Sulu

[20] Protolith ages for two samples are ~2.5 Ga and the best constrained ages from the remaining samples are ~818 Ma to ~728 Ma; the significance of these ages is discussed in a subsequent section. The Mesozoic metamorphic zircon recrystallization ages are more difficult to evaluate because the limited amount of recrystallization gravely restricts the opportunities for measuring spot ages, the measured $^{238}U/^{206}Pb$ ratios have a large spread, the $^{207}Pb/^{206}Pb$ ratios have large uncertainties, and concordia has minimal curvature in the Mesozoic. Sample 94MY08A gave the best constrained age, from 15 equivalent and concordant isotopic ratios, of 229.5 ± 2.6 Ma. Three other samples (99SMC6, 95HZ14A, DPC2) gave equivalent spot ages, but also older and younger ages that we have argued above reflect incomplete recrystallization and subsequent Pb loss, respectively. Thus, from our new data set, 229.5 ± 2.6 Ma is the best age for the UHP metamorphism in Sulu.

4.2. Sm/Nd Age of the UHP Metamorphism

[21] Sm/Nd ages afford the advantage that grains known to be stable only at high pressure can be analyzed to form an isochron. There are now about two dozen Sm/Nd ages from Dabie-Sulu. Table S2 shows all of these isochrons that have MSWD values less than expected for the population size [*Wendt and Carl*, 1991]; as noted in Table S2, some ages have been recalculated using Isoplot. About half are two-point isochrons for which isotopic equilibrium among the constituent grains cannot be assessed, but about half are composed of 3 or more phases such that it is possible to assess equilibrium. Figure 9 (bottom) shows that these ages span a 36 Myr range from 246 ± 6 Ma to 210 ± 9 Ma, with a distribution that suggests four subpopulations of ~240 Ma, ~228 Ma, ~220 Ma and ~212 Ma, regardless of whether one considers the entire data set, only the two-point ages, or only the three-point ages, and regardless of whether one computes weighted mean ages or median ages. The ages of these peaks are clearly influenced to an uncertain extent by the finite number of data, but they bear importantly on the questions posed earlier. Which of these ages are credible? Do these subpopulations signify discrete (re)crystallization events at high pressure?

[22] The oldest three-point age is from a garnet pyroxenite and might be a mixed age reflecting an older history [cf. *Brueckner et al.*, 1996]. If so, one might consider eliminating the "240 Ma" data set from further consideration; we will see below, however, that the existence of this age group is supported by similarly old zircons. A few localities (italicized in Figure 9) have yielded both Sm/Nd and Rb/Sr ages, which can help assess whether the Sm/Nd ages are credible, based on the expectation that the Sm/Nd ages should be older than the Rb/Sr ages: (1) From Zhubian in Sulu, *Li et al.* [1994] reported a Sm/Nd age of 228.5 ± 8.6 Ma and a muscovite Rb/Sr age of 223.9 ± 0.9 Ma; at Qinglongshan (Sulu) their Sm/Nd age is 226.5 ± 9.7 Ma and their phengite Rb/Sr age is 219.5 ± 0.5 Ma. (2) From Shuanghe in Dabie, *Chavagnac et al.* [2001] reported Sm/Nd ages of 238 ± 4 and 229 ± 4 Ma; from the same locale, *Li et al.* [2000] measured Sm/Nd ages of 241.9 ± 3.2, 226.5 ± 3.2 and 226.3 ± 3.2 Ma, and a Rb/Sr phengite age of 219.0 ± 6.6 Ma. (3) From Huangzhen in Dabie, *Li et al.* [2004] reported a multipoint Sm/Nd age of 236.1 ± 8.4 Ma and a Rb/Sr age of 230 ± 14 Ma. (4) From Bixiling in Dabie, *Chavagnac and Jahn* [1996] measured eight Sm/Nd ages from 225 ± 7 Ma to 210 ± 9 Ma and Rb/Sr phengite ages of 214 ± 6 Ma, 212 ± 5, and 198 ± 4 Ma. Four of these Sm/Nd ages, from 215 to 210 Ma, are essentially two-point isochrons as the whole rock and clinopyroxene separates have nearly identical Sm/Nd. This observation, combined with a phengite age as old as 214 Ma, suggests that at Bixiling the oldest, seven-point Sm/Nd age of 225 ± 7 Ma is the best approximation of the age of the eclogite-facies event and that the younger Sm/Nd ages have been reset by subsequent events. This interpretation is also supported by the Bixiling U/Pb zircon data discussed below and suggests that the "212 Ma" Sm/Nd data set reflects post-UHP resetting. In aggregate, this reasoning implies that throughout Sulu and Dabie the best Sm/Nd constraints on the age(s) of the UHP event(s) are the three-point isochrons older than ~225 Ma (the youngest Sm/Nd age with a corresponding Rb/Sr age) or older than ~225–219 Ma (the older Rb/Sr ages).

4.3. Zircon Age of the UHP Metamorphism and the Amphibolite-Facies Overprint

[23] U/Pb zircon ages measured from eclogite, eclogite-bearing gneiss, and garnet peridotite from the UHP terranes of Dabie and Sulu are summarized in Figure 9 and Table S3. To facilitate comparison with the data of this study, and to screen out low-quality analyses, all the SIMS zircon ages in Table S3 are concordia ages (in the sense of *Ludwig* [1998]) from common-Pb corrected concordant spot analyses only; for some data sets this resulted in rejection of a large number of spot ages.

[24] The inferred metamorphic recrystallization ages range from 246 ± 10 Ma to 202.4 ± 2.7 Ma and can be broken into three subpopulations of ~239 Ma, ~226 Ma, and ~216 Ma (Figure 9). The ages of these peaks are median ages computed by weighting all of the ages equally; the weighted mean ages of these same peaks are not significantly different, but are unduly dominated by single high-precision analyses. The peak ages are influenced to an uncertain extent by the finite number of data; their uncertainties, in particular, have limited geologic significance because of the size of the data set.

[25] The ~239 Ma group of zircon ages includes results from two separate studies of rocks from Shuanghe (Dabie), and from two different studies of rocks from Shima (Dabie). This, combined with (1) the fact that the Sm/Nd ages from Shuanghe are the same as the zircon ages and ~10 Myr older than elsewhere (see above) and (2) zircon-inclusion textures described below, lends considerable confidence to the interpretation that the 239 Ma group of zircon ages represents (re)crystallization at UHP. The middle, 226 Ma, group of U/Pb zircon ages is split away from younger ages because (1) a series of post-UHP shoshonitic plutons that

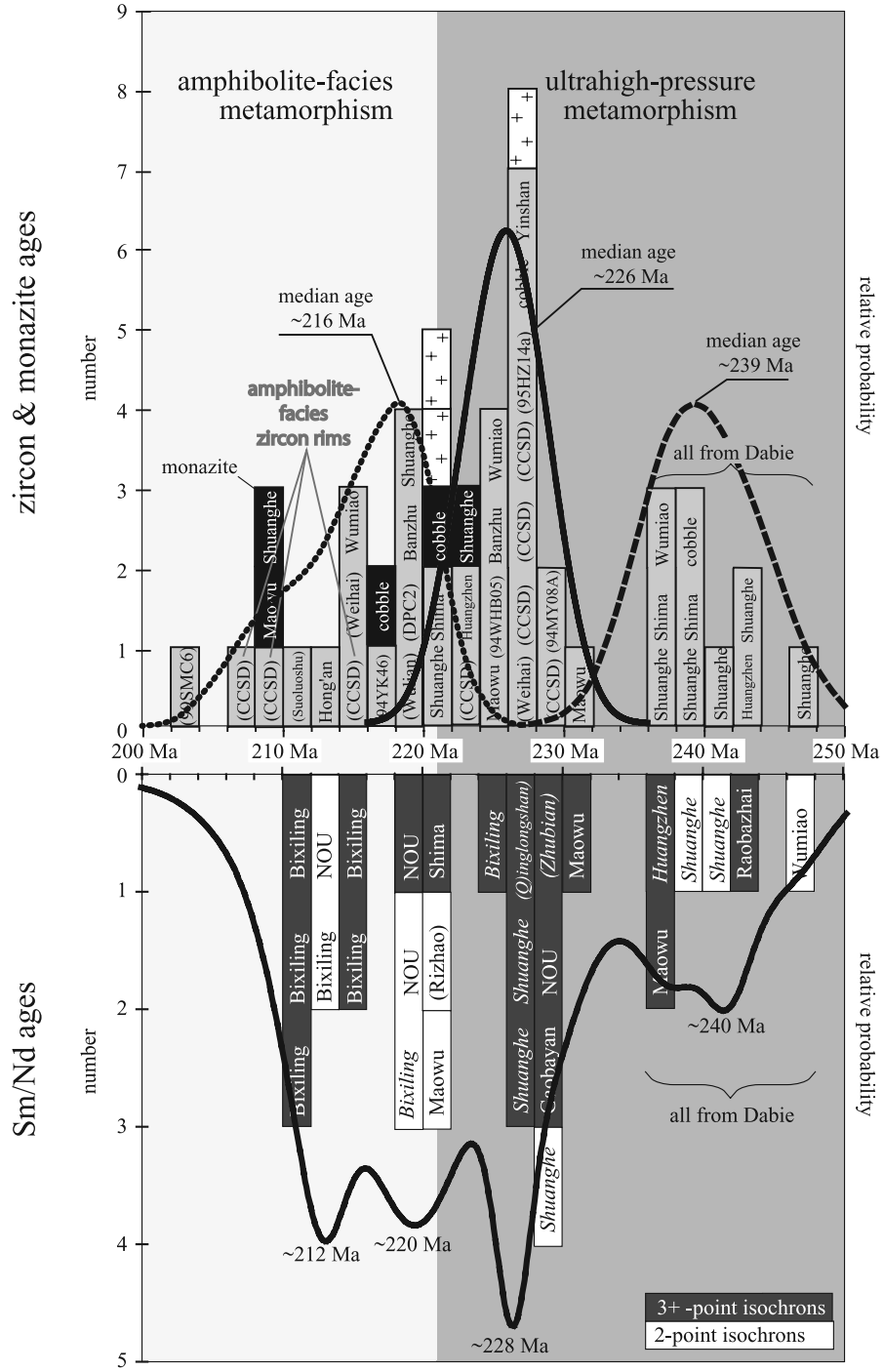

Figure 9. Triassic high-temperature geochronology of the Dabie-Sulu area interpreted to indicate UHP metamorphism in Dabie from ~244 to 236 Ma, an interregnum of 5 Myr, UHP metamorphism in Dabie and Sulu from 230 to 220 Ma, and overprinting amphibolite-facies metamorphism from ~220 to ~205 Ma. Rocks from Sulu are shown in parentheses. (top) Zircon (gray) and monazite (black) ages. Ages on post-UHP igneous suite are white. Probability distribution functions created using equal weighting of all analyses. (bottom) Sm/Nd ages. Ages with corresponding younger Rb/Sr white mica ages are shown in italic. Two-point and three-point or more isochrons are shown in darkening shades of gray. NOU, Northern Orthogneiss Unit.

intrude the UHP gneiss in NE Sulu have crystallization ages of 226–220 Ma (special ornament in Figure 9) [*Chen et al.*, 2003b; *Yang et al.*, 2005a], (2) strongly deformed potassic dikes of a similar age are interpreted to be associated with the UHP metamorphism [*Wallis et al.*, 2005], and (3) a cobble from northern Dabie contains zircons with coesite-bearing mantles dated as ~239 Ma and coesite-bearing rims dated as ~226 Ma [*Wan et al.*, 2005]. The 226 Ma age group comes from both Dabie and Sulu and corresponds to the ~228 Ma group of Sm/Nd ages.

[26] The 216 Ma group of ages comes mostly from localities of similar geographic distribution to the 226 Ma group of ages, although three come from more westerly parts of Dabie (Banzhu and Hong'an in Figure 9). Four observations suggest that the 216 Ma group of zircon ages represents amphibolite-facies (re)crystallization after the UHP metamorphism. (1) A sample from Dabie (Wumiao) consists of 238–220 Ma metamorphic zircons overgrown by 220–214 Ma rims developed at amphibolite facies [*Maruyama et al.*, 1998]. (2) Five samples from Sulu (Donghai) have coesite-bearing zircon domains with ages of 242–220 Ma and quartz-bearing zircon domains with ages of 219–205 Ma [*F. Liu et al.*, 2004a, 2004b, 2005]. (3) A series of 226 to 220 Ma shoshonitic plutons intrude the UHP gneiss in NE Sulu [*Chen et al.*, 2003b; *Yang et al.*, 2005a]. (4) We interpreted the difference between our SIMS + ICP age of 227.1 ± 2.7 Ma and SIMS age of 217.3 ± 4.2 Ma for UHP gneiss 94MY08A to reflect rim Pb loss, although the agreement of this "Pb-loss" age with the zircon overgrowth ages of Maruyama et al. and Liu et al. may be coincidental. If this reasoning that the 216 Ma group of U/Pb zircon ages reflects post-UHP amphibolite-facies metamorphism is correct, the Sm/Nd ages that are younger than ~220 Ma therefore also reflect local amphibolite-facies reequilibration.

4.4. Summary of the Radiochronology of the UHP Rocks

[27] In combination, the Sm/Nd and U/Pb data indicate (1) UHP eclogite-facies recrystallization in the Dabie Shan, but not in Sulu, at ~244–236 Ma; (2) UHP recrystallization at ~230–220 Ma in Dabie and in Sulu; and (3) amphibolite-facies recrystallization beginning at ~220 Ma and continuing on down to ~205 Ma in both Dabie and Sulu. This is the first giant UHP terrane for which a significant span in ages has been documented; equivalent or longer times spans have been documented a UHP domain of unknown size in the northeast Greenland Caledonides [*McClelland et al.*, 2006]. This surprisingly long time span could be the result of (1) daughter-product inheritance, (2) daughter-product loss, (3) multiple subduction events of the same unit, (4) multiple subduction events of different tectonic units, or (5) a long residence time at UHP conditions. We now assess these possibilities in detail.

[28] 1. It is reasonable to imagine that the 244–236 Ma zircon ages might be artifacts produced by incomplete resetting of inherited (e.g., 750 Ma) grains by the 230–220 Ma event, because the technique we employed of using only concordia ages for SIMS data has the potential to skew such ages toward older values because of the minimal curvature in concordia and the large uncertainty in SIMS $^{207}Pb/^{206}Pb$ measurements. One could argue that the 244–236 Ma Sm/Nd ages are similarly too old because of the presence of older inclusions. However, these explanations are unlikely simply because the Sm/Nd and U/Pb ages both show a very similar range from 246 Ma or 244 Ma to 236 Ma, followed by a distinct interregnum of ~5 Myr.

[29] 2. Is the 230–220 Ma "event" an artifact produced by variable daughter-product loss induced by an amphibolite-facies overprint of a 244–236 Ma UHP event? This possibility is more difficult to discount. Because some Sm/Nd ages derived from (U)HP minerals are as young as 211–210 Ma, a time that we know produced amphibolite-facies zircon (re)crystallization, all the Sm/Nd ages might be too young. Moreover, the zircon ages form a continuum from ~231 Ma down to ~209 Ma, suggesting Pb loss or protracted recrystallization. In contrast, the preservation of UHP zircon domains of different ages, 239 Ma and 226 Ma [*Wan et al.*, 2005], combined, again, with the ~5 Myr separation in age between the 244–236 Ma and 230–220 Ma groups, implies that the 230–220 Ma ages reflect a real UHP event.

[30] 3. If we accept that the data require two separate periods of recrystallization at UHP conditions separated by a minimum of ~5 Myr and an average of ~12–13 Myr, one possible explanation is that two distinct tectonic units were subjected to UHP conditions at different times. This explanation can be ruled out, however, because the same area in Dabie that recorded the 244–236 Ma event also has given younger zircon and Sm/Nd ages.

[31] 4. Alternatively, a single tectonic unit in Dabie may have been subjected multiple times to UHP conditions. At present there are no data that allow this hypothesis to be evaluated.

[32] 5. Finally, could a single terrane be subjected to UHP conditions for 12–13 Myr, with different portions of the unit recording various periods of UHP recrystallization? This is unlikely if the terrane remained in the footwall of the subduction zone because even a relatively slow subduction rate of 50 mm/yr would lead to a pressure increase of 5–20 GPa in 12–13 Myr, and a subduction rate of 20 mm/yr would be too slow for most of the plate to avoid heating to mantle temperatures (the characteristic diffusion distance for 12–13 Myr is ~20 km). A more promising scenario for a lengthy period of recrystallization at UHP conditions would be if the subducted terrane were underplated to the hanging wall, refrigerated by ongoing subduction, and then exhumed.

4.5. Diachroneity of the UHP Metamorphism

[33] There is a clear geographic difference between the ages of the eclogite-facies events in Dabie and Sulu. The oldest precise Sm/Nd and U/Pb ages from Sulu are 228.5 ± 8.6 Ma and 228.4 ± 2.4 Ma, respectively, whereas there are 16 ages from Dabie that are significantly older (Figure 9). Many of the older ages come from the Shuanghe or Maowu-Shima-Huangzhen areas in Dabie (Table S2). This implies

that this area was either the first to (re)crystallize at UHP or suffered the least resetting.

4.6. Devonian or Carboniferous Eclogite in Sulu?

[34] In addition to the well-known Triassic UHP and HP eclogites of the Qinling-Dabie-Sulu orogen, eclogites with Paleozoic ages have been discovered in Qinling and Dabie [*Ratschbacher et al.*, 2006]. Coesite- and diamond-bearing eclogites in western Dabie (Hong'an) yielded U/Pb zircon SHRIMP ages of 507 ± 37 Ma and 511 ± 35 Ma [*Yang et al.*, 2003a] and a Sm/Nd garnet-hornblende-omphacite-rutile–whole rock age of 400 ± 16 Ma [*Hu et al.*, 1996]. Ages of ~315 Ma have also been determined from eclogites in this area [*Jian et al.*, 1997, 2001; *Gao et al.*, 2002; *Sun et al.*, 2002; *X. Liu et al.*, 2004]. *Ratschbacher et al.* [2003] suggested that these pre-Triassic UHP metamorphism(s) resulted from aborted subduction of a "Qinling microcontinent" beneath the Sino-Korean craton and from Devonian-Triassic subduction south of that microcontinent. Eclogites of these ages have not been found in Sulu, but we argue below that the Qinling microcontinent is preserved in Sulu.

4.7. Location of the Suture

[35] Significant differences in the tectonic histories of the Sino-Korean and Yangtze cratons mean that the ages of inherited zircons (Figure 10) can be used to determine the location of the suture within Sulu, as was done for Dabie [*Hacker et al.*, 1998] and for the entire Qinling-Dabie orogen [*Ratschbacher et al.*, 2003] (Figure 11). The Sino-Korean Craton consists of two Archean blocks separated by the early Proterozoic Trans-North China Orogen, overprinted by arcs and rifts at its southern and northern margins [e.g., *Kusky and Li*, 2003; *Wilde et al.*, 2004]. Precambrian U/Pb zircon ages of the Sino-Korean Craton cluster at ~3.8 Ga, 3.4–3.0 Ga, and 2.2–2.0 Ga, with the bulk of the ages at ~2.5 Ga (99 data with a mean at ~2502 Ma) and 1.9–1.75 Ga (21 data with a mean at ~1805 Ma) (Figure 10a). The latter two events characterize the Wutai-Fuping arc system and the final assembly of the Sino-Korean Craton, respectively [e.g., *Guan et al.*, 2002; *Wilde et al.*, 2004]. The Sino-Korean Craton was then affected by early Paleozoic (~480 to 400 Ma) arc formation and orogeny along its southern margin (Figure 10a) [*Ratschbacher et al.*, 2003, 2006].

[36] In contrast, the Precambrian U/Pb zircon ages of the Yangtze Craton cluster at 3.3–2.9 Ga, 2.0–1.7 Ga, and ~1.0 Ga, with the majority of the ages at 0.85–0.65 Ga (105 data with a mean at ~755 Ma, Figure 10b). The Neoproterozoic ages most likely date two distinct events that are difficult to separate based only on age. Most of the dated rocks have not been characterized geochemically, but 13 ages from petrochemically well-studied arc rocks along the northern and western Yangtze Craton (Panxi-Hannan arc of *Zhou et al.* [2002]) and the suture between the Yangtze and Cathaysia (Huanan Block) cratons [e.g., *Li*, 1999] give a mean age of ~817 Ma (Figure 10c). The younger event (~732 Ma for 23 well-studied rocks) corresponds to rifting of Rodinia [*Gao et al.*, 1990; *Li et al.*, 1995, 1999] (Figure 10c). These age groups are also found in the Yangtze Craton outside the Qinling-Dabie-Sulu orogen (Figure 10c) [*Qiu et al.*, 2000; *Grimmer et al.*, 2003]. In summary, the Neoproterozoic arc and rifting magmatism are diagnostic of the Yangtze Craton (Figures 10b and 10c), and the Sino-Korean Craton is best recognized by the ~480 to 400 Ma arcs and orogenies that affected its southern edge (Figures 10a and 10e) [*Ratschbacher et al.*, 2003].

[37] On the basis of the identification of retrogressed eclogites and similarities in structural orientation and kinematics, *Faure et al.* [2001, 2003] suggested that the Shandong Peninsula northwest of the YQW fault is part of the Yangtze Craton and was affected by the Triassic UHP metamorphism. Retrogressed eclogites crop out within the Sino-Korean Craton ~500 km west of Sulu [*Zhao et al.*, 2001], however, so the presence of eclogites does not signal Yangtze craton per se. A better test is to use zircon ages. The most common Precambrian zircon ages in Sulu and Dabie are circa 750 Ma, and such ages clearly occur southeast and northwest of the YQW fault in Sulu (Figures 1 and 10d). The Neoproterozoic ages northwest of the YQW fault come from gneissic granites interpreted to constitute the lower part of the Wulian Group, from inherited zircons in Jurassic-Cretaceous gold-bearing granites, and from detrital grains in carbonates (Figure 10d) [*Wang et al.*, 1998; *Zhang et al.*, 2003; *Zhou et al.*, 2003; *Wu et al.*, 2004; *Tang et al.*, 2006]. These ages, combined with the absence of early Paleozoic (~480–400 Ma) ages characteristic of the arcs and orogenies along the southern margin of the Sino-Korean Craton, demonstrate that the Wulian Group is part of the Yangtze Craton.

[38] As discussed above, we interpret our monazite and zircon data (as well as that of *Ishizaka et al.* [1994]) from the gneissic migmatites beneath the Wulian-Fenzishan-Penglai groups northwest of the YQW fault to indicate (re)crystallization events at ~2.7–2.5 Ga and ~1.9 Ga that were only weakly overprinted by a Phanerozoic metamorphism; this contrasts with the strong Triassic UHP and amphibolite-facies metamorphism SE of the YQW fault. In addition, SIMS U/Pb zircon ages obtained by *Faure et al.* [2003] from two samples of the host gneiss to the retrogressed-eclogite(?) boudins are in this same age range. *Ishizaka et al.* [1994] obtained a 1.81 Ga Rb/Sr whole rock age on this host gneiss, and *Zhai et al.* [2000] dated three high-pressure granulites from this area, obtaining Sm/Nd ages of ~1.85, 1.75, and 1.74 Ga. Ages of ~2.5, 2.0, and 1.8 also occur as inherited components in the Jurassic-Cretaceous granites of the Shandong Peninsula (Figure 10d) [*Wang et al.*, 1998; *Zhang et al.*, 2003]. Ages of both 2.5 Ga and 1.8 Ga coincide with the ages of known granulite-facies events in the Sino-Korean Craton [*Zhai et al.*, 2000] and suggest that the gneissic migmatite unit is part of the Sino-Korean Craton. However, both age groups also occur in the Yangtze Craton (Figure 10b), though not in granulites, and thus do not unambiguously tie the gneissic migmatite unit to the Sino-Korean Craton. In addition, one upper intercept age (our sample 95YZB01) and three lower intercept ages of foliated migmatite [*Faure et al.*, 2003] hint at a ~775 Ma event in gneissic migmatites. Thus the gneissic migmatite unit requires further dating to define its provenance.

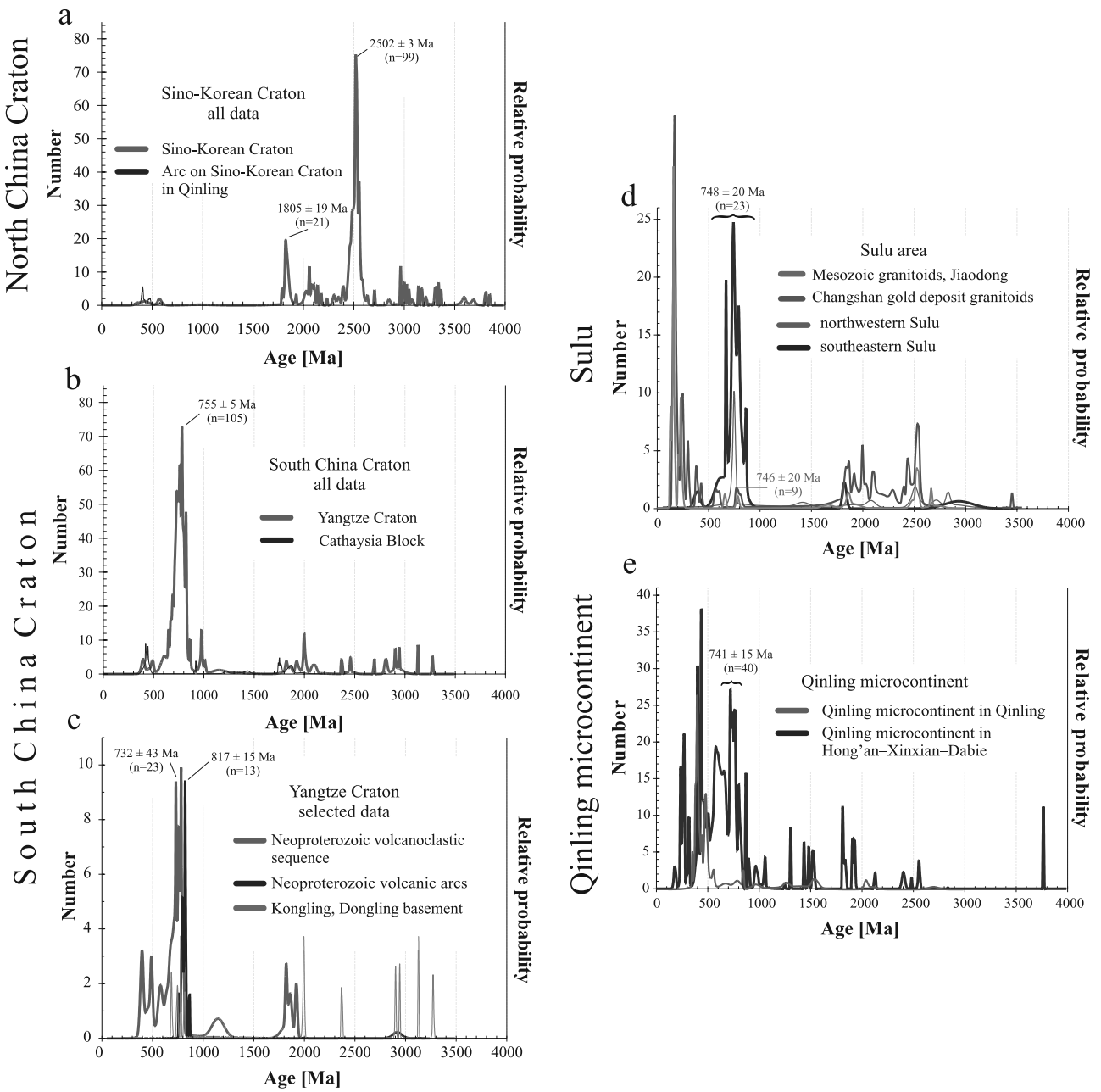

Figure 10. Pre-Triassic zircon ages from the (d) Sulu area compared to (a) the Sino-Korean Craton and the Ordovician-Devonian arc along its southern margin (arc data only from Qinling). (b) Data from the South China Craton split into the two major blocks. (c) Yangtze craton data, divided based on geotectonic setting and region. (e) Data of the Qinling microcontinent. Data in Figure 10d are from the compilation by *Ratschbacher et al.* [2006].

[39] There are three possible ways to explain the geology of northwestern Sulu in terms of Sino-Korean versus Yangtze affinity.

[40] 1. The Wulian-Fenzishan-Penglai groups are parts of the Yangtze Craton thrust northwestward over Sino-Korean basement (the gneissic migmatite); this would place the Triassic suture along the YQW, as in most current tectonic models. *Wallis et al.* [1999] and *Faure et al.* [2003] demonstrated top NW kinematics throughout Sulu, but that deformation is due to exhumation, rather than crustal thickening.

[41] 2. The entire northwestern Sulu area is part of the Yangtze Craton, and the Triassic suture lies northwest of Sulu. The relationship of the Wulian-Fenzishan-Penglai groups to the gneissic migmatite in Sulu resembles that observed in Dabie between the volcaniclastic Changpu and Ganghe "cover units" and the depositionally underlying "Yangtze basement gneisses"; that cover is dated at ~761 Ma

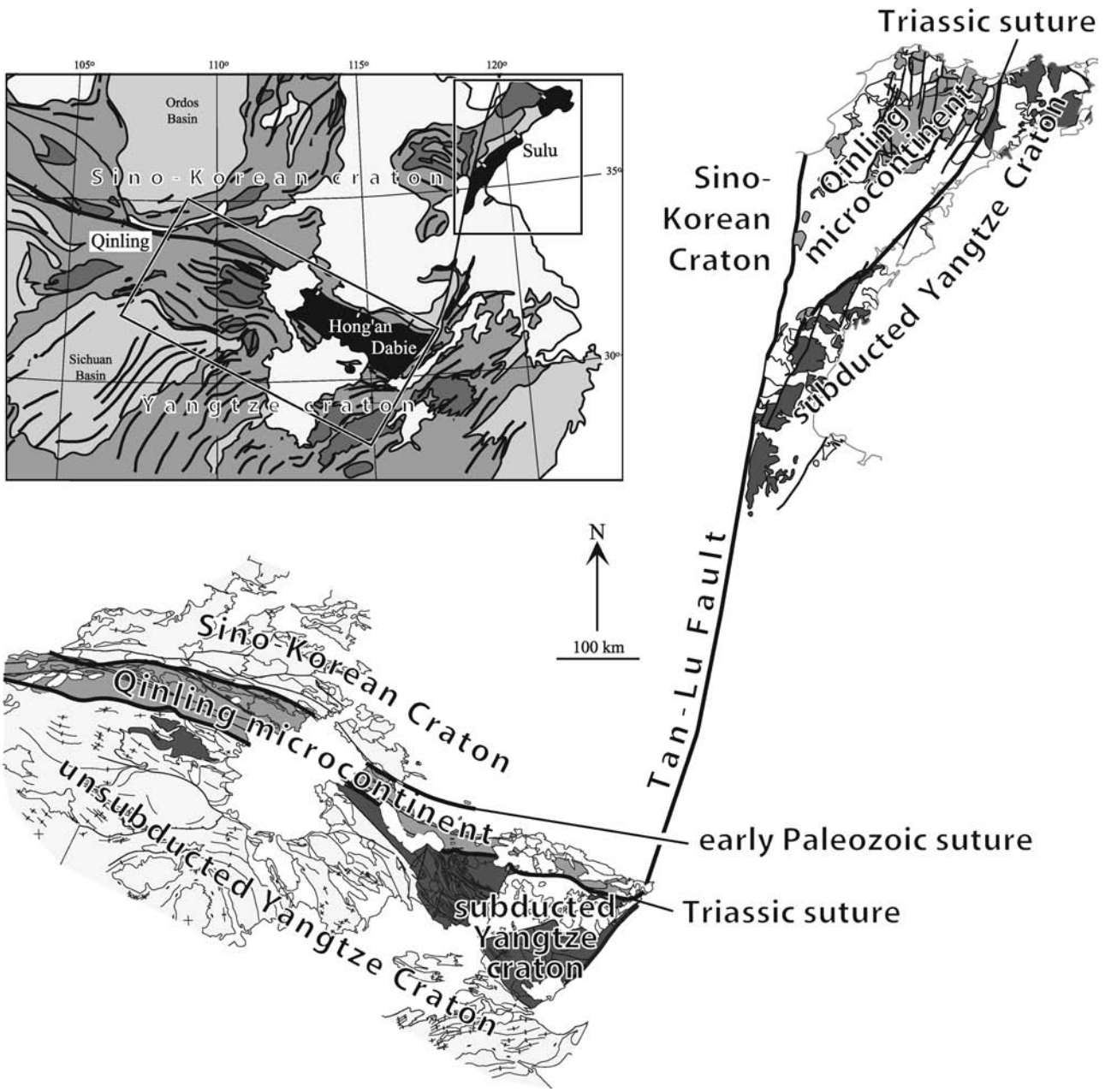

Figure 11. Architecture of the Qinling-Dabie-Sulu orogen, emphasizing how the once subducted UHP portion of the Yangtze craton is separated from the Sino-Korean hanging wall by the Qinling ribbon microcontinent. Rock units younger than Triassic are unshaded.

(U/Pb zircon) and was interpreted as part of the Neoproterozoic rift sequence of the Yangtze Craton [*Oberhänsli et al.*, 2002; *Schmid et al.*, 2003]. Unfortunately, the basement gneisses are undated and poorly characterized, prohibiting a direct comparison with the gneissic migmatite of northwestern Sulu. Ages of ~2.5 Ga and ~1.8 Ga occur in Dabie but cannot be clearly associated with "Yangtze gneisses" beneath the Neoproterozoic rift sequence. Speculatively, an orthogneiss at Bixiling with a 2458 ± 76 Ma upper intercept SIMS zircon age (sample CF96-39 of *Chavagnac et al.* [2001]), close to the study area of *Schmid et al.* [2003] and a granulite within the northern Orthogneiss Unit in northern Dabie with a 2456 ± 7 Ma Pb/Pb zircon evaporation age may constitute the closest Dabie equivalents to the gneissic migmatite in Sulu.

[42] In Dabie, the Triassic suture between the Yangtze and Sino-Korean cratons does not coincide with the northern boundary of the UHP-HP rocks, but actually lies 10–50 km farther north, such that the Sino-Korean Craton and the UHP part of the Yangtze Craton are separated by an unsubducted part of the Yangtze Craton (Luzhenguang Complex [*Hacker et al.*, 1998; *Chen et al.*, 2003a; *Hacker et al.*, 2004]). It is possible that a similar situation exists in Sulu: the Wulian-Fenzishan-Penglai groups and probably the gneissic migma-

tite units correspond to this unsubducted part of the Yangtze Craton. In this model, the UHP-HP rocks of the Qinling-Dabie-Sulu orogen developed by intracontinental subduction and exhumation.

[43] 3. We prefer a third scenario that resolves controversies about the age of the Sino-Korean/Yangtze Craton collision (Figure 11). We propose that there was an early Paleozoic collision between the Qinling microcontinent and the southern margin of the Sino-Korean Craton, and then a Triassic collision of this collage with the Yangtze Craton [*Ratschbacher et al.*, 2006]. The Qinling microcontinent is a long and narrow ribbon continent that extends at least through Qinling and Dabie. Here we suggest that it continues into Sulu and constitutes the basement and cover north of the YQW fault. In Qinling and Dabie, the Qinling microcontinent is characterized by the ~1.0 Ga Jinningian orogeny, ~0.8–0.7 Ga arc formation and rifting, and ~470–400 Ma arc formation (Figure 10) [*Ratschbacher et al.*, 2006]. Thus the Qinling microcontinent's Proterozoic history ties it to the Yangtze Craton, from which it rifted at ~0.75 Ga when Rodinia broke apart (see above). Its Paleozoic arc, mid-late Paleozoic fore-arc basin, and its separation from the Yangtze Craton by an oceanic mélange, render the Qinling microcontinent distinct [*Ratschbacher et al.*, 2006].

[44] How does this scenario apply to Sulu? The Wulian Group has already been correlated lithologically with the Luzhenguang and Foziling complexes of Dabie [*Zhou et al.*, 2002]. The basal sections are both ~0.75 Ga gneissic granites [*Zhou et al.*, 2002; *Chen et al.*, 2003a] and are intercalated with and/or overlain by a mafic series in the Wulian Group and in the Luzhenguang complex (where it is ~0.75 Ga [*Hacker et al.*, 2000]). The "upper" part of the Wulian Group is quartzite, carbonaceous slate, phyllite, and marble. The Foziling complex in Dabie consists of marble overlain by monotonous siliciclastic rocks interpreted as a forearc sequence [*Ratschbacher et al.*, 2006]. Migmatites are rare in the Luzhenguang and have not been dated, however, detrital zircon ages of 1.5, 1.8–1.9, and 2.5 Ga in the Foziling and Luzhenguang groups [*Chen et al.*, 2003a] suggest that basement with ages similar to the gneissic migmatite of Sulu was present in the hinterland. In summary, we propose that the migmatitic basement in Sulu is the basement of the Qinling microcontinent, and the Wulian Group is the Neoproterozoic cover (which has Sinian fossils [*Zhou et al.*, 1995]) of that microcontinent plus an overlying forearc sequence.

[45] Where is the 470–400 Ma arc in Sulu? Such arc rocks are ubiquitous as plutons in Qinling and represented by volcanic rocks in northern Hong'an (Figure 10e), but occur in Dabie only as recycled detritus in the fore-arc basin rocks. Thus the arc may not have been present or may have undergone greater exhumation in the east. The $\leq 70^{\circ}$ counterclockwise rotation of the Sino-Korean Craton with respect to the Yangtze Craton during collision [*Zhao and Coe*, 1987; *Gilder et al.*, 1999] implies that the intervening Paleotethys ocean narrowed eastward, perhaps restricting arc formation in the east.

5. Conclusions

[46] New U/Pb zircon and U-Th/Pb ages from monazite were presented from the Sulu UHP domain. Our best zircon determination of the UHP event in Sulu is 229.5 ± 2.6 Ma; the monazite ages are insufficiently reset and not helpful in determining the age(s) of the UHP metamorphism. All Triassic Sm/Nd ages and all U/Pb zircon ages from the Sulu and Dabie UHP terranes fall in three groups. The ~230–220 Ma group of ages is considered the "main" UHP event, based on (1) inclusion relationships in zircons, (2) the absence of older Rb/Sr ages, and (3) the presence of a 226–220 Ma post-UHP intrusive suite, and the agreement between U/Pb and Sm/Nd ages. Younger ages of ~220–205 Ma represent amphibolite-facies recrystallization, based on (1) inclusion relationships in zircons; (2) the association, in some samples, with higher U concentrations in the younger ages; (3) the patterns of older Rb/Sr ages, (4) the presence of a 226–220 Ma post-UHP intrusive suite, and (5) the fact that many of the Sm/Nd ages are younger than the U/Pb ages. The oldest group of ages, 244–236 Ma, come exclusively from Dabie. The distinct time gap between these ages and the 230–220 Ma peak implies two distinct UHP recrystallization events. Widespread ~750 Ma zircons, reveal that like the Dabie Shan, a low-pressure crustal sliver of Yangtze affinity was trapped north of the deeply subducted part of the Yangtze Craton in Sulu and escaped subduction.

[47] **Acknowledgments.** Samples used in this study were collected during JSPS projects awarded to S. Banno, T Hirajima, and S Wallis. Analytical work was funded by projects Ra442/19 of the Deutsche Forschungsgemeinschaft and NSF grants EAR-9796119, EAR-9725667, and EAR-0003568. Thoughtfully and thoroughly reviewed by James Connelly and David Root.

References

Ames, L., G. Zhou, and B. Xiong (1996), Geochronology and geochemistry of ultrahigh-pressure metamorphism with implications for collision of the Sino-Korean and Yangtze cratons, central China, *Tectonics*, *15*, 472–489.

Banno, S., M. Enami, T. Hirajima, A. Ishiwatari, and Q. Wang (2000), Decompression P-T path of coesite eclogite to granulite from Weihai, eastern China, *Lithos*, *52*, 97–108.

Brueckner, H. K., J. Blusztajn, and N. Bakun-Czubarow (1996), Trace element and Sm-Nd 'age' zoning in garnets from peridotites of the Caledonian and Variscan Mountains and tectonic implications, *J. Metamorph. Geol.*, *14*, 61–73.

Chavagnac, V., and B.-M. Jahn (1996), Coesite-bearing eclogites from the Bixiling Complex, Dabie Mountains, China; Sm-Nd ages, geochemical characteristics and tectonic implications, *Chem. Geol.*, *133*, 29–51.

Chavagnac, V., B.-M. Jahn, I. M. Villa, M. Whitehouse, and D. Liu (2001), Multichronometric evidence for an in situ origin of the ultrahigh-pressure metamorphic terrane of Dabieshan, *China, J. Geol.*, *109*, 633–646.

Chen, F., J.-H. Guo, L.-L. Jiang, W. Siebel, B. Cong, and M. Satir (2003a), Provenance of the Beihuaiyang lower-grade metamorphic zone of the Dabie ultrahigh-pressure collisional orogen, China: Evidence from zircon ages, *J. Asian Earth Sci.*, *22*, 343–352.

Chen, J.-F., Z. Xie, H. M. Li, X. Zhang, T.-X. Zhou, D. G. Chen, X. D. Zhang, Y. X. Park, and K. S. Ahn (2003b), U-Pb zircon ages for a collision-related K-rich complex at Shidao in the Sulu ultrahigh pressure terrane, China, *Geochem. J.*, *37*, 36–46.

Enami, M., K. Suzuki, M. Zhai, and X. Zheng (1993), The chemical Th-U-total Pb isochron ages of Jiaodong and Jiaonan metamorphic rocks in the Shandong Peninsula, eastern China, *Island Arc*, *2*, 104–113.

Faure, M., W. Lin, and N. Le Breton (2001), Where is the North China–South China block boundary in eastern China?, *Geology*, *29*, 119–122.

Faure, M., W. Lin, P. Monié, N. Le Breton, S. Poussineau, D. Panis, and E. Deloule (2003), Exhumation tectonics of the ultrahigh-pressure metamorphic rocks in the Qinling orogen in east China: New petological-structural-radiometric insights from the Shandong Peninsula, *Tectonics*, *22*(3), 1018, doi:10.1029/2002TC001450.

Gao, S., B. R. Zhang, and Z. J. Li (1990), Geochemical evidence for Proterozoic continental arc and continental margin rift magmatism along the northern margin of the Yangtse craton, south China, *Precambrian Res.*, *47*, 205–221.

Gao, S., Y. Qiu, W. Ling, N. J. McNaughton, B. Zhang, G. Zhang, Z. Zhang, Z. Zhong, and S. Suo (2002), SHRIMP single zircon U-Pb geochronology of eclogites from Yingshan and Xiongdian, *Earth Sci. J. China Univ. Geosci. Wuhan*, *27*, 558–564.

Gilder, S. A., P. H. Leloup, V. Courtillot, Y. Chen, R. Coe, X. Zhao, W. Xiao, N. Halim, J.-P. Cogne, and R. Zhu (1999), Tectonic evolution of the Tancheng-Lujiang (Tan-Lu) fault via Middle Triassic to Early Cenozoic paleomagnetic data, *J. Geophys. Res.*, *104*, 15,365–15,390.

Grimmer, J. C., L. Ratschbacher, L. Franz, I. Gaitzsch, M. Tichomirowa, M. McWilliams, and B. R. Hacker (2003), When did the ultrahigh-pressure rocks reach the surface? A $^{207}Pb/^{206}Pb$ zircon, $^{40}Ar/^{39}Ar$ white mica, Si-in-phengite single grain study of Dabie Shan synorogenic foreland sediments, *Chem. Geol.*, *197*, 87–110.

Guan, H., M. Sun, S. A. Wilde, X. Zhou, and M. Zhai (2002), SHRIMP U-Pb zircon geochronology of the Fuping Complex: Implications for formation and assembly of the North China Craton, *Precambrian Res.*, *113*, 1–18.

Hacker, B. R., T. Sharp, R. Y. Zhang, J. G. Liou, and R. L. Hervig (1997), Determining the origin of ultrahigh-pressure lherzolites, *Science*, *258*, 702–704.

Hacker, B. R., L. Ratschbacher, L. Webb, T. Ireland, D. Walker, and S. Dong (1998), U/Pb zircon ages constrain the architecture of the ultrahigh-pressure Qinling-Dabie Orogen, China, *Earth Planet. Sci. Lett.*, *161*, 215–230.

Hacker, B. R., L. Ratschbacher, L. E. Webb, M. McWilliams, T. R. Ireland, A. Calvert, S. Dong, H.-R. Wenk, and D. Chateigner (2000), Exhumation of ultrahigh-pressure continental crust in east-central China: Late Triassic–Early Jurassic tectonic unroofing, *J. Geophys. Res.*, *105*, 13,339–13,364.

Hacker, B. R., L. Ratschbacher, and J. G. Liou (2004), Subduction, collision, and exhumation in the Qinling-Dabie Orogen, *J. Geol. Soc. London*, *226*, 157–175.

Hoskin, P. W. O., and U. Schaltegger (2003), The composition of zircon and igneous and metamorphic petrogenesis, in *Zircon*, *Rev. Mineral. Geochem.*, vol. 53, edited by J. M. Hanchar and P. W. O. Hoskin, pp. 27–62, Mineral. Soc. of Am., Washington, D. C.

Hu, N., J. Yang, and D. Zhao (1996), Sm-Nd isochron age of eclogite from northern Qinling Mountains, *Acta Mineral. Sin.*, *16*, 349–352.

Ishizaka, K., T. Hirajima, and X. S. Zheng (1994), Rb-Sr dating for the Jiaodong gneiss of the Su-Lu ultrahigh pressure province, eastern China, *Island Arc*, *3*, 232–241.

Jian, P., W. Yang, Z. C. Li, and H. Zhou (1997), Isotopic geochronological evidence for the Caledonian Xiongdian eclogite in the western Dabie mountains, China, *Acta Geol. Sin.*, *10*, 455–465.

Jian, P., D. Liu, W. Yang, and I. S. Williams (2001), SHRIMP dating of zircons from the Caledonian Xiongdian eclogite, western Dabie Mountains, China, *Chin. Sci. Bull.*, *46*, 77–79.

Kato, T., M. Enami, and M. Zhai (1997), Ultrahigh-pressure (UHP) marble and eclogite in the Su-Lu UHP terrane, eastern China, *J. Metamorph. Geol.*, *15*, 169–182.

Kusky, T. M., and J. Li (2003), Paleoproterozoic tectonic evolution of the North China Craton, *J. Asian Earth Sci.*, *22*, 383–397.

Leech, M. L., L. E. Webb, and T. N. Yang (2006), Diachronous histories for the Dabie-Sulu orogen from high-temperature geochronology, in *Ultrahigh-Pressure Metamorphism: Deep Continental Subduction*, edited by B. R. Hacker, W. C. McClelland, and J. G. Liou, *Spec. Pap. Geol. Soc. Am.*, *403*, 1–22.

Li, S., Y. Xiao, D. Liou, Y. Chen, N. Ge, Z. Zhang, S.-S. Sun, B. Cong, R. Zhang, S. R. Hart, and S. Wang (1993), Collision of the north China and Yangtze blocks and formation of coesite-bearing eclogites: Timing and processes, *Chem. Geol.*, *109*, 89–111.

Li, S., S. Wang, Y. Chen, D. Liu, J. Qiu, H. Zhou, and Z. Zhang (1994), Excess argon in phengite from eclogite: Evidence from the dating of eclogite minerals by the Sm-Nd, Rb-Sr and $^{40}Ar/^{39}Ar$ methods, *Chem. Geol.*, *112*, 343.

Li, S., E. Jagoutz, Y. Chen, and Q. Li (2000), Sm-Nd and Rb-Sr isotopic chronology and cooling history of ultrahigh pressure metamorphic rocks and their country rocks at Shuanghe in the Dabie Mountains, central China, *Geochim. Cosmochim. Acta*, *64*, 1077–1093.

Li, X.-H. (1999), U-Pb zircon ages of granites from the southern margin of the Yangtze Block: Timing of Neoproterozoic Jinning Orogeny in SE China and implications for Rodinia assembly, *Precambrian Res.*, *97*, 43–57.

Li, X.-P., Y.-F. Zheng, Y.-B. Wu, F. Chen, B. Gong, and Y.-L. Li (2004), Low-T eclogite in the Dabie terrane of China: Petrological and isotopic constraints on fluid activity and radiometric dating, *Contrib. Mineral. Petrol.*, *148*, 443–470.

Li, Z.-X., L. Zhang, and C. M. Powell (1995), South China in Rodinia: Part of the missing link between Australia–East Antarctica and Laurentia, *Geology*, *23*, 407–410.

Li, Z. X., X. H. Li, P. D. Kinny, and J. Wang (1999), The breakup of Rodinia: Did it start with a mantle plume beneath south China?, *Earth Planet. Sci. Lett.*, *173*, 171–181.

Liou, J. G., and R. Y. Zhang (1996), Occurrence of intergranular coesite in ultrahigh-P rocks from the Sulu region, eastern China: Implications for lack of fluid during exhumation, *Am. Mineral.*, *81*, 1217–1221.

Liu, F., Z. Xu, J. G. Liou, and B. Song (2004a), SHRIMP U-Pb ages of ultrahigh-pressure and retrograde gneisses, southwestern Sulu terrane, eastern China, *J. Metamorph. Geol.*, *22*, 315–326.

Liu, F., Z. Xu, and H. Xue (2004b), Tracing the protolith, UHP metamorphism, and exhumation ages of orthogneiss from the SW Sulu terrane (eastern China): SHRIMP U-Pb dating of mineral inclusion-bearing zircons, *Lithos*, *78*, 411–429.

Liu, F., J. G. Liou, and Z. Xu (2005), U-Pb SHRIMP ages recorded in the coesite-bearing zircon domains of paragneisses in the southwestern Sulu terrane, eastern China: New interpretation, *Am. Mineral.*, *90*, 790–800.

Liu, X., B.-M. Jahn, D. Liu, S. Dong, and S. Li (2004c), SHRIMP U-Pb zircon dating of a metagabbro and eclogites from western Dabieshan (Hong'an Block), China, and its tectonic implications, *Tectonophysics*, *394*, 171–192.

Ludwig, K. R. (1998), On the treatment of concordant uranium-lead ages, *Geochim. Cosmochim. Acta*, *62*, 665–676.

Maruyama, S., H. Tabata, A. P. Nutman, T. Morikawa, and J. G. Liou (1998), SHRIMP U-Pb geochronology of ultrahigh-pressure metamorphic rocks of the Dabie Mountains, central China, *Cont. Dyn.*, *3*, 72–85.

Mattinson, C. G., R. Y. Zhang, T. Tsujimori, and J. G. Liou (2004), Epidote-rich talc-kyanite-phengite eclogites, Sulu terrane, eastern China: P-T-f_{O2} estimates and the significance of the epidote-talc assemblage in eclogite, *Am. Mineral.*, *89*, 1772–1783.

McClelland, W. C., S. E. Power, J. A. Gilotti, F. K. Mazdab, and B. Wopenka (2006), U-Pb SHRIMP geochronology and trace-element geochemistry of coesite-bearing zircons, North-East Greenland Caledonides, in *Ultrahigh-Pressure Metamorphism: Deep Continental Subduction*, edited by B. R. Hacker, W. C. McClelland, and J. G. Liou, *Spec. Pap. Geol. Soc. Am.*, *403*, 23–43.

Nakamura, D., and T. Hirajima (2000), Granulite-facies overprinting of ultrahigh-pressure metamorphic rocks, northeastern Sulu region, eastern China, *J. Petrol.*, *41*, 563–582.

Oberhänsli, R., G. Martinotti, R. Schmid, and X. Liu (2002), Preservation of primary volcanic textures in the ultrahigh-pressure terrain of Dabie Shan, *Geology*, *30*, 609–702.

Proyer, A., E. Dachs, and C. McCammon (2004), Pitfalls in geothermobarometry of eclogites: Fe3+ and changes in the mineral chemistry of omphacite at ultrahigh pressures, *Contrib. Mineral. Petrol.*, *147*, 305–318.

Qiu, Y. M., S. Gao, N. J. McNaughton, D. I. Groves, and W. Ling (2000), First evidence of >3. 2 Ga continental crust in the Yangtze craton of south China and its implications for Archean crustal evolution and Phanerozoic tectonics, *Geology*, *28*, 11–14.

Ratschbacher, L., B. R. Hacker, A. Calvert, L. E. Webb, J. C. Grimmer, M. McWilliams, T. R. Ireland, S. Dong, and J. Hu (2003), Tectonics of the Qinling (central China): Tectonostratigraphy, geochronology, and deformation history, *Tectonophysics*, *366*, 1–53.

Ratschbacher, L., C. Dingeldey, C. Miller, B. R. Hacker, and M. O. McWilliams (2004), Formation, subduction, and exhumation of Penninic oceanic crust in the eastern Alps: Time constraints from $^{40}Ar/^{39}Ar$ geochronology, *Tectonophysics*, *394*, 155–170.

Ratschbacher, L., L. Franz, E. Enkelmann, R. Jonckheere, A. Pörschke, B. R. Hacker, S. Dong, and Y. Zhang (2006), The Sino-Korean-Yangtze suture, the Huwan detachment, and the Paleozoic-Tertiary exhumation of (ultra)high-pressure rocks along the Tongbai-Xinxian-Dabie, in *Ultrahigh-Pressure Metamorphism: Deep Continental Subduction*, edited by B. R. Hacker, W. C. McClelland, and J. G. Liou, *Spec. Pap. Geol. Soc. Am.*, *403*, 45–75.

Regional Geological Survey of Jiangsu (1984), *Regional Geology of Jiangsu Province and Shanghai Municipality*, 857 pp., Geol. Publ. House, Beijing.

Regional Geological Survey of Shandong (1991), *Regional Geology of Shandong Province*, 595 pp., Geol. Publ. House, Beijing.

Rolfo, F., R. Compagnoni, W. Wu, and S. Xu (2004), A coherent lithostratigraphic unit in the coesite–eclogite complex of Dabie Shan, China: Geologic and petrologic evidence, *Lithos*, *73*, 71–94.

Schmid, R., R. L. Romer, L. Franz, R. Oberhänsli, and G. Martinotti (2003), Basement-cover sequences within the UHP unit of the Dabie Shan, *J. Metamorph. Geol.*, *21*, 531–538.

Sun, W., I. S. Williams, and S. Li (2002), Carboniferous and Triassic eclogites in the western Dabie Mountains, east-central China: Evidence for protracted convergence of the North and South China Blocks, *J. Metamorph. Geol.*, *20*, 873–886.

Tang, J., Y.-F. Zheng, Y.-B. Wu, and B. Gong (2006), Zircon SHRIMP U-Pb dating, C and O isotopes for impure marbles from the Jiaobei terrane in the Sulu orogen: Implication for tectonic affinity, *Precambrian Res.*, *144*, 1–18.

Wallis, S. R., A. Ishiwatari, T. Hirajima, K. Ye, J. Guo, D. Nakamura, K. Kato, M. Zhai, M. Enami, B. Cong, and S. Banno (1997), Occurrence and field relationships of ultrahigh-pressure metagranitoid and coesite eclogite in the Su-Lu terrane, eastern China, *J. Geol. Soc. London*, *154*, 45–54.

Wallis, S. R., M. Enami, and S. Banno (1999), The Sulu UHP terrane: A review of the petrology and structural geology, *Int. Geol. Rev.*, *41*, 906–920.

Wallis, S., M. Tsuboi, K. Suzuki, J. Laili, and T. Tanaka (2005), Role of partial melting in the evolution of the Sulu UHP terrane, *Geology*, *33*, 129–132.

Wan, Y., R. Li, S. A. Wilde, D. Liu, Z. Chen, L. Yan, T. Song, and X. Yin (2005), UHP metamorphism and exhumation of the Dabie Orogen, China: Evidence from SHRIMP dating of zircon and monazite from a UHP granitic gneiss cobble from the Hefei Basin, *Geochim. Cosmochim. Acta*, *69*, 4333–4348.

Wang, L. G., Y. M. Qiu, N. J. McNaughton, D. I. Groves, Z. K. Luo, J. Z. Huang, L. C. Miao, and Y. K. Liu (1998), Constraints on crustal evolution and gold metallogeny in the northwestern Jiaodong Peninsula, China, from SHRIMP U-Pb zircon studies of granitoids, *Ore Geol. Rev.*, *13*, 275–291.

Wendt, I., and C. Carl (1991), The statistical distribution of the mean squared weighted deviation, *Chem. Geol.*, *86*, 275–285.

Wilde, S. A., P. A. Cawood, K. Wang, A. Nemchin, and G. Zhao (2004), Determining Precambrian crustal evolution in China: A case study from Wutaishan, Shanxi Province, demonstrating the application of precise SHRIMP U-Pb geochronology, in *Aspects of the Tectonic Evolution of China*, edited by J. Malpas et al., pp. 5–25, Geol. Soc., London.

Wu, Y., Y. Zheng, and J. Zhou (2004), Neoproterozoic granitoid in northwest Sulu and its bearing on the North China–South China blocks boundary in east China, *Geophys. Res. Lett.*, *31*, L07616, doi:10.1029/2004GL019785.

Yang, J., Z. Xu, L. F. Dobrzhinetskaya, H. W. Green II, X. Pei, R. Shi, C. Wu, J. L. Wooden, J. Zhang, J. Wan, and H. Li (2003a), Discovery of metamorphic diamonds in central China: An indication of a >4000–km-long zone of deep subduction resulting from multiple continental collisions, *Terra Nova*, *15*, 370–379.

Yang, J. S., J. L. Wooden, C. L. Wu, F. L. Liu, Z. Q. Xu, R. D. Shi, I. Katayama, J. G. Liou, and S. Maruyama (2003b), SHRIMP U-Pb dating of coesite-bearing zircon from the ultrahigh-pressure metamorphic rocks, Sulu terrane, east China, *J. Metamorph. Geol.*, *21*, 551–560.

Yang, J.-H., S.-L. Chung, S. A. Wilde, F.-Y. Wu, M.-F. Chu, C.-H. Lo, and H.-R. Fan (2005a), Petrogenesis of post-orogenic syenites in the Sulu Orogenic Belt, east China: Geochronological, geochemical and Nd–Sr isotopic evidence, *Chem. Geol.*, *214*, 99–125.

Yang, J.-H., F.-Y. Wu, S.-L. Chung, S. A. Wilde, M.-F. Chu, C.-H. Lo, and B. Song (2005a), Petrogenesis of Early Cretaceous intrusions in the Sulu ultrahigh-pressure orogenic belt, east China and their relationship to lithospheric thinning, *Chem. Geol.*, *222*, 200–231.

Zhai, M., B. Cong, J. Guo, W. Liu, Y. Li, and Q. Wang (2000), Sm-Nd geochronology and petrography of garnet pyroxene granulites in the northern Sulu region of China and their geotectonic implication, *Lithos*, *52*, 23–33.

Zhang, R., J. G. Liou, and W. G. Ernst (1995), Ultrahigh-pressure pressure metamorphism and decompressional P-T paths of eclogites and country rocks from Weihai, eastern China, *Island Arc*, *4*, 293–309.

Zhang, R. Y., and J. G. Liou (1998), Ultrahigh-pressure metamorphism of the Sulu Terrane, eastern China: A perspective view, *Cont. Dyn.*, *3*, 32–53.

Zhang, X., P. A. Cawood, S. A. Wilde, R. Liu, H. Song, W. Li, and L. W. Snee (2003), Geology and timing of mineralization at the Canghang gold deposit, north-western Jiaodong peninsula, China, *Mineral. Deposita*, *38*, 141–153.

Zhao, G., P. A. Cawood, S. A. Wilde, and L. Liangzhao (2001), High-pressure granulites (retrograded eclogites) from the Hengshan Complex, North China Craton: Petrology and tectonic implications, *J. Petrol.*, *42*, 1141–1170.

Zhao, X. X., and R. S. Coe (1987), Palaeomagnetic constraints on the collision and rotation of north and south China, *Nature*, *327*, 141–144.

Zhou, D., L. Cheng, and M. Liu (1995), The discovery of solenopora in the Wulian group in the Jiaonian area, Shandong, and its significance, *Reg. Geol. China*, *14*, 379–384.

Zhou, J.-B., Y.-F. Zheng, and Y.-B. Wu (2003), Zircon U-Pb ages for Wulian granites in northwest Sulu and their tectonic implications, *Chin. Sci. Bull.*, *48*, 379–384.

Zhou, M.-F., A. K. Kennedy, M. Sun, J. Malpas, and C. M. Lesher (2002), Neoproterozoic arc-related mafic intrusions along the northern margin of south China: Implications for the accretion of Rodinia, *J. Geol.*, *110*, 611–618.

G. Gehrels, Department of Geosciences, University of Arizona, Gould-Simpson Building 77, 1040 E 4th St., Tucson, AZ 85721, USA.

M. Grove, Department of Earth and Space Sciences, University of California, Los Angeles, 595 Charles Young Drive East, Box 951567, Los Angeles, CA 90095-1567, USA.

B. R. Hacker, Department of Geological Sciences, University of California, Santa Barbara, CA 93106-9630, USA. (hacker@geol.ucsb.edu)

L. Ratschbacher, Institut für Geowissenschaften, Technische Universität Bergakademie Freiberg, Bernhard-von-Cottastr.2, D-09596 Freiberg/Sachsen, Germany.

S. R. Wallis, Department of Earth and Planetary Sciences, Graduate School of Environmental Studies, Nagoya University, Nagoya 464-8602, Japan.

Data Repository

Analytical Methods

Zircon and monazite were separated using standard gravity and magnetic separation techniques. Grains of different sizes were placed in separate epoxy mounts; the mounts were polished variably—some enough to expose grain cores and some just enough to expose only the grain surface to enable analysis of metamorphic rims, which tended to be <10 μm wide. Cathodoluminescent images of all zircons were then obtained with a JEOL 6300 scanning electron microscope and a home-built imaging system at UC Santa Barbara and interpreted using techniques similar to Corfu et al. [71]. All monazite U-Th-Pb work was performed with the GV Isoprobe multi-collector inductively coupled plasma (ICP) mass spectrometer at the University of Arizona, using a laser to ablate the grains. The zircon U-Pb analyses were obtained using this instrument and the Cameca IMS-1270 secondary-ion mass spectrometer (SIMS) at UCLA. These two instruments were used in tandem to exploit the advantages of each: the Isoprobe excavates larger volumes of material (see below), minimizing problems with surface contamination and the effects of inclusions, and can rapidly analyze a large number of grains; whereas SIMS has greater spatial resolution, necessary when working on grains with narrow metamorphic overgrowths. For all ages we report 95% confidence-interval uncertainties that include errors in decay constants unless stated otherwise. Isotopic ratios were corrected for common lead using a ^{204}Pb correction and the model of Stacey and Kramers [72]. Three different sessions on the IMS-1270 used normal operating procedures [73, 74] and zircon AS3 [75] as a standard.

The University of Arizona Isoprobe is equipped with 9 faraday collectors, an axial Daly detector, and 4 ion-counting channels. A New Wave (Merchantek) 193 nm ArF laser system was operated in 20-sec long bursts at 32 mJ, a repetition rate of 8 Hz and spot sizes of 35 or 50 μm to ablate ~15 μm deep pits in zircon; monazites were analyzed at a repetition rate of 4 Hz and a spot size of 10 μm. The ablated material was transported to the ICP using a mixture of Ar and He carrier gases where it underwent ‘dry’ nebulization. The carrier gases have sufficiently low Hg abundance that any Hg in the 204 mass position was subtracted by measuring on-peak backgrounds prior to sample analysis. Mass 204 was measured using an ion-counting channel whereas masses 206, 207, 208, 232 and 238 were measured with Faraday detectors; all analyses were conducted in static mode. Each blank and unknown measurement consisted of 20 separate 1-second counts. Because the measured isotopic ratios generally vary as a function of increasing laser pit depth, their values corresponding to a ‘zero pit depth’ were determined by regression of the ratio-vs.-time data, using an Excel macro written by Gehrels and Hacker. The regression was iterative, with ratios differing from their expected value by more than 3 sigma being rejected sequentially until the line was a good fit to all data. Fits that showed no statistically significant slope with respect to pit depth were recomputed with the

slope forced to zero. Subsequent data reduction and plotting were done with Isoplot [76].

Mass fractionation on the Isoprobe was established by analyzing zircon and monazite standards of known ages after every few unknowns. For our 564-Ma Sri Lankan zircon standard with 461 ppm U and 457 ppm Th, typical counting-measurement errors (2σ) are 206/238 = 1.8%, 206/207 = 8%, and 208/232 = 6%. The expected/measured fractionation factors (2σ) for the zircon standard are 206/238: 1.276 ± 0.072, 206/207: 1.016 ± 0.034, and 208/232: 0.802 ± 0.128. These two sources of measurement error for the 206/238 ratio, 1.8% and 5.6%, respectively, dominate the internal error of the $^{206}Pb/^{238}U$ age (the common-Pb correction contributes only ~0.18% uncertainty, as measured 206/204 ratios are typically >3500). The choice of common-Pb correction, the 0.107% uncertainty in the ^{238}U decay constant, and the 0.7% uncertainty in the age of the standard lead to ~0.82% (2σ) additional error in the absolute $^{238}U/^{206}Pb$ age. The two sources of measurement error for the 206/207 ratio, 8% and 6.6%, respectively, dominate the internal error of the $^{207}Pb/^{206}Pb$ age (the common-Pb correction contributes ~1.2% uncertainty, as measured 207/204 ratios are typically >300). The choice of common-Pb correction, the 0.136% uncertainty in the ^{238}U decay constant, and the 0.7% uncertainty in the age of the standard cause ~0.8% (2σ) additional error in the absolute $^{207}Pb/^{206}Pb$ age. Thus, a single analysis of our 564-Ma zircon standard typically has a precision of ±33.2 Ma (2σ) and an accuracy of ±33.5 Ma (2σ) in the $^{238}U/^{206}Pb$ age, and ±58.8 Ma (2σ) and ±59.1 Ma (2σ) in the $^{207}Pb/^{206}Pb$ age. Ten analyses of the same zircon grain enable improvements in the accuracy of the $^{238}U/^{206}Pb$ age to ± 11.5 Ma and of the $^{207}Pb/^{206}Pb$ age to ± 19.1 Ma (2 standard errors of the mean). Both SIMS and ICP ages are corrected using ^{204}Pb; because the $^{206}Pb/^{204}Pb$ ratios are large this has little impact on the ages.

For our 425-Ma monazite standard #44069 [77] typical counting-measurement errors are (2σ) 206/238 = 2.6%, 206/207 = 14%, and 208/232 = 2.4%. The expected/measured fractionation factors (2σ) for the monazite standard are 206/238: 1.35 ± 0.066, 206/207: 0.75 ± 0.10, and 208/232: 0.96 ± 0.03. These two sources of measurement error, 2.4% and 3.2%, respectively for the 208/232 ratio dominate the internal error of the Th/Pb age (the common-Pb correction contributes only ~0.24% uncertainty, as measured 208/204 ratios are typically 1500-2000). The choice of common-Pb correction, the 0.1% uncertainty in the ^{232}Th decay constant, and the 0.7% uncertainty in the age of the standard lead to ~0.74% (2σ) additional error in the absolute age. Thus, a single analysis of our monazite standard typically has a precision of ± 17.0 Ma (2σ) and an accuracy of ± 17.3 Ma (2σ). Ten analyses of the same monazite grain leads to improvements in the precision to ± 5.4 Ma and in the accuracy to ± 6.2 Ma (2 standard errors of the mean).

Table 1. Zircon and monazite U, Th, and Pb isotopic data.

Zircon

Analysis Type	Name[†]	Th/U	U ppm	Th ppm	Age(Ma) $^{206}Pb/^{238}U$[‡]	±1 s.e. (%)	$^{238}U/^{206}Pb^{*}$[‡]	±1 s.e. (%)	$^{207}Pb^{*}/^{206}Pb^{*}$[‡]	±1 s.e. (%)
94MY08A: N36°53.70' E122°30.22'										
ICP	94MY08A-2.14r	0.05	2230	113	205.5	2.7	30.87	2.8	0.0533	5.7
SIMS	94MY08A-9.2	0.01	529	8	210.1	2.3	30.19	2.4	0.0513	4.1
SIMS	94MY08A-8.1	0.01	709	5	214.5	2.2	29.56	2.3	0.0503	4.9
SIMS	94MY08A-3.2	0.05	1222	59	218.7	2.2	28.97	2.2	0.0499	1.9
SIMS	94MY08A-7.1	0.01	318	3	218.8	2.3	28.96	2.4	0.0497	14.6
SIMS	94MY08A-4.1	0.06	618	36	222.0	1.9	28.54	1.9	0.0497	2.9
ICP	94MY08A-4.18r	0.03	1019	27	222.1	2.3	28.52	2.3	0.0528	8.2
ICP	94MY08A-4.7	0.02	870	21	222.6	2.7	28.46	2.7	0.0456	5.6
ICP	94MY08A-3.5	0.02	609	15	222.8	2.5	28.44	2.5	0.0440	10.3
ICP	94MY08A-5.22r	0.02	380	9	223.8	2.6	28.31	2.6	0.0519	13.3
ICP	94MY08A-4.8	0.02	958	21	224.2	2.6	28.26	2.6	0.0459	6.0
ICP	94MY08A-1.11	0.04	258	10	226.4	2.6	27.98	2.7	0.0445	26.8
ICP	94MY08A-3.16r	0.02	547	12	227.0	2.6	27.90	2.7	0.0507	8.3
SIMS	94MY08A-6.2	0.02	733	18	227.2	1.8	27.87	1.9	0.0542	7.8
ICP	94MY08A-4.20r	0.03	941	24	228.0	2.4	27.78	2.4	0.0501	6.4
SIMS	94MY08A-9.1	0.01	559	6	228.9	2.0	27.67	2.1	0.0502	7.2
SIMS	94MY08A-6.1	0.03	859	26	234.3	2.0	27.02	2.1	0.0520	2.9
ICP	94MY08A-2.12r	0.02	482	11	235.1	2.7	26.92	2.7	0.0536	16.7
SIMS	94MY08A-3.1	0.05	1027	47	235.2	1.2	26.92	1.2	0.0506	1.9
SIMS	94MY08A-10.1	0.01	5093	29	235.3	1.8	26.89	1.9	0.0511	1.4
ICP	94MY08A-2.2	0.02	948	15	237.8	2.5	26.62	2.6	0.0448	8.5
ICP	94MY08A-2.13c	0.05	805	43	239.3	2.9	26.44	2.9	0.0558	7.7
SIMS	94MY08A-1.1	0.09	882	80	242.0	1.9	26.14	1.9	0.0554	3.5
SIMS	94MY08A-1.3	0.03	2091	59	252.2	2.1	25.06	2.1	0.0518	4.8
SIMS	94MY08A-4.2	0.05	643	33	261.5	3.4	24.16	3.5	0.0513	2.3
ICP	94MY08A-4.9	0.04	1853	66	286.7	4.0	21.99	4.1	0.0553	5.1
SIMS	94MY08A-1.2	0.10	730	74	298.7	2.7	21.08	2.7	0.0533	4.4
ICP	94MY08A-3.6	0.06	1460	83	299.1	2.5	21.06	2.6	0.0586	5.7
SIMS	94MY08A-2.1	0.11	623	70	368.3	2.2	17.01	2.3	0.0572	1.9
ICP	94MY08A-3.17r	0.37	181	67	379.1	3.2	16.51	3.3	0.0606	15.2
ICP	94MY08-10	0.09	858	77	551.7	2.3	11.19	2.4	0.0659	5.2
SIMS	94MY08A-5.1	0.99	43	42	862.3	6.0	6.99	6.4	0.0700	4.4
94TJP02: N37°12.97' E120°59.42'										
SIMS	94TJP02-5	0.18	212	38	1906.0	1.2	2.91	1.4	0.1203	0.6
SIMS	94TJP02-4	0.31	251	79	2352.2	1.3	2.27	1.6	0.1624	0.4
SIMS	94TJP02-1	0.14	769	110	2396.9	0.7	2.22	0.8	0.1602	0.2
SIMS	94TJP02-7	0.40	297	117	2414.0	1.3	2.20	1.5	0.1620	0.5
SIMS	94TJP02-6	0.35	107	37	2554.5	1.7	2.06	2.0	0.1909	0.8
SIMS	94TJP02-2	0.14	469	64	2596.6	0.9	2.02	1.1	0.1823	0.2
SIMS	94TJP02-3	0.71	310	219	2931.0	1.0	1.74	1.2	0.2063	0.3
ICP	94TJP02-2	0.30	360	108	2400.5	1.4	2.22	1.7	0.1952	4.3
ICP	94TJP02-1	0.53	181	95	2521.8	1.5	2.09	1.8	0.1880	4.4
ICP	94TJP02-4	0.41	528	214	2544.4	1.4	2.07	1.7	0.1879	4.3
ICP	94TJP02-3	0.39	81	31	2767.8	2.3	1.86	2.8	0.1839	5.6
94WHB05: N37°31.08' E122°09.45'										

SIMS	94WHB05-11.1	0.00	101	0	170.5	4.2	37.32	4.3	0.0477	11.2
SIMS	94WHB05-14.1	0.02	48	1	194.1	5.4	32.71	5.5	0.0545	21.9
SIMS	94WHB05-15.1	0.02	121	2	219.4	2.3	28.89	2.3	0.0519	5.4
SIMS	94WHB05-6.1	0.01	1861	26	225.1	1.3	28.14	1.3	0.0507	1.1
SIMS	94WHB05-4.1	0.01	136	2	250.5	4.5	25.24	4.6	0.0476	13.0
SIMS	94WHB05-8.1	0.01	186	1	258.6	4.6	24.43	4.7	0.0539	7.2
SIMS	94WHB05-7.1	0.04	253	9	261.0	3.1	24.21	3.1	0.0484	6.0
SIMS	94WHB05-12.1	0.12	191	23	274.9	3.6	22.95	3.7	0.0539	5.6
ICP	94WHB05-4	0.34	381	76	370.6	2.2	16.90	2.2	0.0504	5.6
ICP	94WHB05-13	0.45	139	68	487.8	3.1	12.72	3.2	0.0601	8.6
SIMS	94WHB05-3.1	0.66	462	304	496.0	1.3	12.50	1.4	0.0615	2.1
ICP	94WHB05-14	0.46	151	75	518.3	3.0	11.95	3.2	0.0585	9.5
ICP	94WHB05-8r	0.24	161	42	519.3	2.4	11.92	2.5	0.0514	19.2
ICP	94WHB05-7c	0.54	142	84	532.2	2.3	11.62	2.4	0.0588	9.4
ICP	94WHB05-19	0.53	369	211	546.0	3.0	11.31	3.1	0.0643	7.2
ICP	94WHB05-18	0.54	765	448	552.6	2.8	11.17	2.9	0.0648	5.2
ICP	94WHB05-6	0.78	569	481	557.8	3.6	11.06	3.8	0.0575	5.8
SIMS	94WHB05-6.2	0.78	268	208	577.0	3.0	10.68	3.1	0.0613	2.0
SIMS	94WHB05-10.1	0.90	228	205	615.8	5.4	9.98	5.6	0.0615	4.4
SIMS	94WHB05-5.1	0.81	128	104	627.8	4.7	9.78	4.9	0.0626	4.3
ICP	94WHB05-5	0.66	166	96	671.8	2.2	9.10	2.3	0.0601	3.1
SIMS	94WHB05-13.1	0.72	211	153	692.6	2.5	8.82	2.6	0.0605	2.7
ICP	94WHB05-11c	0.74	308	263	702.0	2.8	8.69	3.0	0.0617	8.2
SIMS	94WHB05-9.1	0.51	253	130	713.0	2.2	8.55	2.4	0.0618	2.7
ICP	94WHB05-9c	0.77	185	156	719.0	2.6	8.47	2.7	0.0658	9.4
SIMS	94WHB05-11.2	0.72	129	93	719.9	2.9	8.46	3.0	0.0643	3.1
SIMS	94WHB05-2.1	0.78	174	136	742.6	1.9	8.19	2.0	0.0623	2.6
ICP	94WHB05-10r	0.57	202	126	792.2	3.2	7.65	3.4	0.0598	5.6
94YK46: N36°15.07' E120°40.67'										
SIMS	94YK46-9.1	0.00	234	0	209.2	1.4	30.32	1.5	0.0485	4.6
SIMS	94YK46-19.1	0.00	255	1	215.2	1.6	29.45	1.6	0.0474	4.5
SIMS	94YK46-1.1	0.01	524	7	215.8	1.1	29.37	1.1	0.0503	1.5
SIMS	94YK46-15.1	0.01	325	3	216.2	1.2	29.32	1.2	0.0509	3.3
SIMS	94YK46-17.1	0.01	348	4	218.2	1.3	29.05	1.3	0.0504	2.6
SIMS	94YK46-8	0.00	260	1	223.5	1.5	28.35	1.6	0.0529	4.7
SIMS	94YK46-14	0.32	582	188	298.2	1.0	21.12	1.0	0.0553	1.3
SIMS	94YK46-11	0.14	164	24	316.0	1.2	19.90	1.2	0.0578	3.8
SIMS	94YK46-7	0.08	2000	168	322.5	0.9	19.49	0.9	0.0559	1.1
SIMS	94YK46-6	0.16	963	155	329.9	1.0	19.04	1.1	0.0565	1.4
SIMS	94YK46-1.2	0.30	299	88	347.6	1.5	18.05	1.5	0.0559	2.7
SIMS	94YK46-18.1	0.10	234	24	353.3	1.5	17.75	1.5	0.0568	3.2
SIMS	94YK46-12	0.19	373	69	355.2	1.2	17.65	1.3	0.0572	2.0
SIMS	94YK46-3	0.16	392	63	355.6	1.1	17.63	1.1	0.0569	2.6
SIMS	94YK46-4.2	0.36	552	199	494.0	1.1	12.56	1.1	0.0597	1.0
SIMS	94YK46-5	1.02	226	231	506.0	1.0	12.25	1.0	0.0621	1.5
ICP	94YK46-6	0.52	371	193	608.9	3.5	10.09	3.6	0.0598	11.0
SIMS	94YK46-2	0.71	100	71	661.6	1.5	9.25	1.6	0.0643	2.5
SIMS	94YK46-13	0.85	242	206	725.3	1.0	8.40	1.1	0.0646	1.1
SIMS	94YK46-9.2	0.76	120	92	744.2	1.6	8.17	1.6	0.0638	1.9
95HZ14A: N34°29.80' E118°48.12'										
SIMS	95HZ14A-18.1	1.09	839	60	214.5	1.3	29.56	1.3	0.0531	5.0
SIMS	95HZ14A-13.2	0.41	1053	31	225.7	1.2	28.07	1.2	0.0519	1.8
SIMS	95HZ14A-13.3	0.83	993	32	226.5	1.9	27.97	1.9	0.0496	6.0
SIMS	95HZ14A-15.1	2.12	737	47	235.3	1.3	26.89	1.3	0.0526	4.6

SIMS	95HZ14A-17.1	1.09	1162	144	286.9	1.8	21.98	1.8	0.0552	5.5
SIMS	95HZ14A-6.3	1.24	760	412	318.6	2.5	19.74	2.6	0.0560	6.1
SIMS	95HZ14A-13.1	2.24	278	73	411.8	2.1	15.16	2.2	0.0582	7.8
ICP	95HZ14A-15	1.01	301	302	445.5	19.5	13.98	4.5	0.0591	7.3
SIMS	95HZ14A-11.1	1.02	749	358	479.8	4.3	12.94	4.5	0.0642	3.1
SIMS	95HZ14A-16.1	1.51	383	171	523.8	1.2	11.81	1.3	0.0592	2.5
SIMS	95HZ14A-14.1	1.98	351	180	559.2	2.3	11.04	2.4	0.0602	5.7
SIMS	95HZ14A-3	1.46	251	86	656.6	1.0	9.33	1.1	0.0631	1.4
SIMS	95HZ14A-1	1.26	835	725	695.7	0.8	8.78	0.9	0.0651	0.6
SIMS	95HZ14A-7	1.87	169	80	706.2	0.9	8.64	1.0	0.0654	2.2
SIMS	95HZ14A-6.2	1.50	464	257	715.7	1.0	8.52	1.1	0.0657	1.3
ICP	95HZ14A-4	1.26	261	330	718.9	45.3	8.48	6.7	0.0561	11.7
ICP	95HZ14A-20	1.65	816	1348	722.5	8.7	8.43	1.3	0.0661	4.0
SIMS	95HZ14A-12.1	2.83	323	232	731.4	1.1	8.32	1.1	0.0633	3.0
ICP	95HZ14A-5	1.51	733	1104	758.3	21.4	8.01	3.0	0.0641	3.6
ICP	95HZ14A-14	1.47	454	668	761.2	26.8	7.98	3.7	0.0639	6.6
ICP	95HZ14A-16	1.42	301	428	764.6	20.4	7.94	2.8	0.0581	4.9
ICP	95HZ14A-18	1.45	511	743	765.0	49.8	7.94	6.9	0.0639	3.6
SIMS	95HZ14A-10	1.40	311	195	770.1	1.1	7.88	1.2	0.0648	0.9
SIMS	95HZ14A-5.1	1.85	665	463	780.5	1.0	7.77	1.0	0.0633	1.1
SIMS	95HZ14A-9	1.30	324	234	793.6	1.6	7.63	1.7	0.0658	0.8
SIMS	95HZ14A-8	1.60	144	72	796.0	2.0	7.61	2.2	0.0644	2.1
SIMS	95HZ14A-2	1.43	676	510	798.2	0.9	7.59	0.9	0.0648	0.7
SIMS	95HZ14A-5.2	1.30	636	465	804.9	0.9	7.52	1.0	0.0649	0.5
SIMS	95HZ14A-4	1.39	827	579	813.6	0.8	7.43	0.9	0.0648	0.6
95YZB01: N37°06.05' E121°18.43'										
SIMS	95YZB01-5	0.24	383	91	154.4	2.1	41.26	2.1	0.0497	4.4
SIMS	95YZB01-10	0.98	41	41	156.8	4.2	40.62	4.3	0.0448	46.1
SIMS	95YZB01-3	0.81	183	147	159.9	1.6	39.81	1.6	0.0429	18.3
SIMS	95YZB01-1.1	0.03	2938	74	161.5	1.0	39.41	1.0	0.0478	2.2
SIMS	95YZB01-7	0.94	123	115	163.0	3.1	39.06	3.2	0.0426	14.3
SIMS	95YZB01-1.2	0.62	79	49	163.2	2.8	39.01	2.8	0.0499	21.5
SIMS	95YZB01-2	0.52	1402	727	175.2	1.9	36.30	1.9	0.0487	2.3
SIMS	95YZB01-8	0.32	534	168	499.6	2.1	12.41	2.2	0.0618	2.1
SIMS	95YZB01-6	0.65	133	86	713.4	2.4	8.55	2.5	0.0624	7.5
99JP7: N34°31.90' E119°07.70'										
SIMS	99JP7-7	0.39	466	182	359.9	1.7	17.42	1.8	0.0586	3.1
SIMS	99JP7-10.1	0.72	108	78	517.2	2.3	11.97	2.4	0.0650	5.4
SIMS	99JP7-12.1	0.46	56	26	526.6	4.4	11.75	4.5	0.0657	10.5
SIMS	99JP7-9.1	0.74	145	108	553.7	1.9	11.15	2.0	0.0638	3.8
SIMS	99JP7-3.2	0.83	279	232	576.7	1.6	10.69	1.7	0.0641	2.0
SIMS	99JP7-11.1	0.90	62	56	691.7	2.7	8.83	2.9	0.0588	8.2
SIMS	99JP7-5	0.80	130	104	708.9	2.0	8.60	2.1	0.0638	3.3
SIMS	99JP7-4	0.71	70	50	733.1	1.5	8.30	1.6	0.0639	3.0
SIMS	99JP7-2	0.87	12	10	812.4	4.4	7.45	4.6	0.0665	9.2
SIMS	99JP7-6	0.70	62	43	819.3	1.8	7.38	1.9	0.0661	2.7
99SMC6: N37°10.97' E122°02.53'										
SIMS	99SMC6-14.1	0.02	821	14	182.3	1.8	34.87	1.8	0.0497	12.9
SIMS	99SMC6-9.1	0.01	447	3	189.9	2.3	33.45	2.4	0.0435	11.8
ICP	99SMC6-8	0.03	1657	56	195.2	4.2	32.53	4.3	0.0544	5.6
SIMS	99SMC6-2.2	0.01	735	7	196.9	1.7	32.24	1.7	0.0452	12.4
SIMS	99SMC6-13.1	0.02	1690	29	200.9	2.0	31.59	2.0	0.0495	2.8
SIMS	99SMC6-13.2	0.01	2218	33	201.6	1.4	31.49	1.4	0.0501	2.6
ICP	99SMC6-5b	0.04	952	40	204.4	1.3	31.04	1.3	0.0560	5.5

SIMS	99SMC6-8.1	0.02	2865	51	206.5	1.5	30.72	1.5	0.0503	2.2
ICP	99SMC6-1.11r	0.13	227	30	231.4	2.6	27.36	2.6	0.0545	27.4
ICP	99SMC6-17r	0.44	166	72	233.9	4.1	27.06	4.2	0.0528	25.9
SIMS	99SMC6-11.1	0.12	1106	135	242.0	1.4	26.14	1.5	0.0542	3.0
ICP	99SMC6-16r	0.42	81	34	275.1	5.0	22.93	5.1	0.0624	35.1
ICP	99SMC6-4b	0.57	145	83	305.4	3.5	20.61	3.6	0.0554	15.0
ICP	99SMC6-3a	0.10	613	61	318.4	2.6	19.75	2.7	0.0488	7.2
ICP	99SMC6-7r	0.39	182	71	319.2	6.5	19.70	6.7	0.0568	7.9
SIMS	99SMC6-10.1	0.55	102	56	329.9	3.0	19.05	3.1	0.0629	10.5
SIMS	99SMC6-12.1	0.29	1049	302	360.3	1.5	17.40	1.6	0.0574	3.5
ICP	99SMC6-1.12r	0.20	197	39	364.0	5.8	17.22	5.9	0.0695	19.7
SIMS	99SMC6-7.1	0.26	1178	303	400.6	1.9	15.60	2.0	0.0573	1.5
ICP	99SMC6-9r	0.40	475	192	402.2	3.1	15.53	3.2	0.0606	6.2
ICP	99SMC6-14r	0.75	81	60	420.0	3.9	14.85	4.0	0.0516	34.8
SIMS	99SMC6-5.1	0.63	32	20	490.3	5.5	12.65	5.7	0.0685	15.7
SIMS	99SMC6-3.1	0.39	233	91	547.0	3.0	11.29	3.1	0.0619	2.4
ICP	99SMC6-13c	0.79	94	74	559.8	8.6	11.02	8.9	0.0573	19.4
ICP	99SMC6-1b	0.90	57	51	566.4	2.9	10.89	3.1	0.0545	22.1
SIMS	99SMC6-7.2	0.51	617	317	669.9	2.3	9.13	2.5	0.0627	1.2
SIMS	99SMC6-3.2	0.84	53	45	696.4	5.3	8.77	5.6	0.0704	2.5
SIMS	99SMC6-1.1	0.76	536	410	717.9	2.1	8.49	2.2	0.0661	2.5
SIMS	99SMC6-2.3	0.75	85	64	731.3	4.1	8.32	4.4	0.0678	4.3
ICP	99SMC6-3b	0.64	150	96	749.9	1.7	8.11	1.8	0.0595	6.2
SIMS	99SMC6-2.1	1.10	49	53	846.3	26.1	7.13	27.9	0.0612	13.7
DPC2: N35°52.75' E119°27.18'										
SIMS	DPC2-4.1	0.02	724	17	196.6	2.0	32.29	2.1	0.0512	4.5
SIMS	DPC2-5.1	0.03	689	18	199.4	2.2	31.84	2.2	0.0493	2.9
SIMS	DPC2-7.1	0.03	809	27	202.2	1.4	31.38	1.4	0.0506	2.1
SIMS	DPC2-6.2	0.03	657	19	204.6	1.4	31.01	1.4	0.0511	2.3
SIMS	DPC2-7.2	0.03	1111	34	206.1	1.4	30.79	1.5	0.0488	3.3
SIMS	DPC2-9.2	0.02	547	11	207.1	2.6	30.63	2.7	0.0526	2.4
SIMS	DPC2-9.1	0.02	631	13	210.7	2.8	30.10	2.8	0.0524	2.1
SIMS	DPC2-8.1	0.03	750	20	211.4	1.9	30.00	1.9	0.0501	2.3
SIMS	DPC2-15.1	0.73	173	127	215.6	1.2	29.41	1.2	0.0493	1.6
SIMS	DPC2-12.1	0.61	268	164	216.8	1.2	29.24	1.2	0.0516	1.5
SIMS	DPC2-16.1	0.52	635	332	216.9	1.2	29.22	1.2	0.0494	2.3
SIMS	DPC2-2.1	0.02	636	14	219.1	1.8	28.93	1.8	0.0521	3.7
SIMS	DPC2-8.2	0.02	579	12	219.1	1.9	28.92	1.9	0.0492	1.9
SIMS	DPC2-6.1	0.03	808	25	219.5	1.2	28.87	1.3	0.0510	3.4
SIMS	DPC2-11.1	0.03	1131	36	223.4	2.1	28.36	2.1	0.0501	2.6
SIMS	DPC2-2.2	0.03	560	15	226.0	1.5	28.03	1.5	0.0501	5.3
SIMS	DPC2-10.1	1.27	245	311	477.7	2.2	13.00	2.2	0.0600	3.8
SIMS	DPC2-1.1	0.96	107	103	756.4	3.4	8.03	3.6	0.0627	4.4
SIMS	DPC2-8.3	2.25	24	54	806.0	5.4	7.51	5.7	0.0585	10.5
DZ7: N37°17.63' E121°08.47										
SIMS	DZ7-2.1	0.69	322	222	1632.3	1.6	3.47	1.8	0.1147	1.1
SIMS	DZ7-5.1	0.67	588	397	1651.4	1.2	3.42	1.3	0.1136	1.2
SIMS	DZ7-1.1	0.62	872	545	1741.4	2.8	3.22	3.2	0.1180	1.6
SIMS	DZ7-4.1	0.52	166	87	1867.5	2.6	2.98	2.9	0.1266	1.5
ICP	DZ7-2	0.37	311	117	2406.2	2.6	2.21	2.6	0.1683	5.5
ICP	DZ7-3	0.67	538	359	2440.3	2.7	2.17	2.7	0.1680	4.5
ICP	DZ7-6	0.47	478	223	2442.0	2.6	2.17	2.6	0.1555	3.2
ICP	DZ7-4	0.66	187	124	2515.8	2.7	2.09	2.7	0.1669	6.7

ICP	DZ7-1	0.55	235	129	2558.0	2.5	2.05	2.5	0.1581	5.0
ICP	DZ7-5	0.66	290	192	2578.0	2.6	2.03	2.6	0.1640	4.5

Monazites

Analysis Type†	Name	Th/U	U ppm	Th ppm	Age (Ma) $^{208}Pb^*/^{232}Th$‡	±1 s.e. (%)	$^{208}Pb^*/^{232}Th$ ‡	±1 s.e. (%)
92HH1: N37°02.73' E120° 40.12'								
ICP	92HH1-5	10.7	56	592	346.9	12.4	0.02	3.62
ICP	92HH1-1.2	14.9	35	515	430.8	14.4	0.02	3.37
ICP	92HH1-1.4	4.1	51	212	612.2	31.5	0.03	5.23
ICP	92HH1-10	30.4	71	2149	747.9	33.6	0.04	4.57
ICP	92HH1-6	24.2	79	1901	1278.4	27.0	0.07	2.18
ICP	92HH1-1	16.3	103	1680	1439.7	19.4	0.07	1.40
ICP	92HH1-11	16.0	445	7106	1775.6	24.2	0.09	1.43
ICP	92HH1-12	14.6	348	5062	1807.0	20.8	0.09	1.20
ICP	92HH1-9	17.2	446	7690	1819.6	43.7	0.09	2.51
ICP	92HH1-8	11.8	585	6876	1849.8	23.0	0.10	1.30
ICP	92HH1-7	11.9	310	3691	1880.1	21.6	0.10	1.20
92HXS05: N37° 21.07' E120°10.30'								
ICP	92HXS05-4	8.7	653	5647	1681.5	35.2	0.09	2.18
ICP	92HXS05-5	10.0	159	1598	1782.9	24.8	0.09	1.45
ICP	92HXS05-3	10.1	754	7590	1826.2	44.7	0.09	2.56
ICP	92HXS05-2	8.7	919	7963	2010.8	30.1	0.10	1.57
ICP	92HXS05-1	9.2	750	6924	2043.9	32.5	0.11	1.67
92KB1: N37°10.17' E120°46.90'								
ICP	92KB1-3.10	10.5	587	6172	676.5	20.2	0.03	3.04
ICP	92KB1-3.11	17.7	437	7731	882.8	15.5	0.04	1.80
ICP	92KB1-9	10.5	206	2150	1743.1	92.4	0.09	5.53
ICP	92KB1-2.6	12.3	189	2331	1806.0	46.6	0.09	2.70
ICP	92KB1-1.2	6.9	692	4794	1808.2	40.5	0.09	2.34
ICP	92KB1-1.1	6.9	544	3730	1843.0	69.9	0.10	3.97
ICP	92KB1-12	10.1	674	6824	1854.7	32.6	0.10	1.84
ICP	92KB1-2.4	8.4	453	3784	1860.8	53.6	0.10	3.01
ICP	92KB1-1.3	16.1	263	4244	1877.5	47.5	0.10	2.65
ICP	92KB1-5.16	8.8	724	6404	1884.1	41.2	0.10	2.29
ICP	92KB1-2.5	7.9	430	3417	1884.6	47.1	0.10	2.62
ICP	92KB1-5.17	11.1	630	7010	1891.0	50.0	0.10	2.77
ICP	92KB1-7	9.7	382	3695	1920.7	37.4	0.10	2.04
ICP	92KB1-8	11.0	440	4821	1976.8	38.6	0.10	2.05
ICP	92KB1-4.14	10.4	291	3022	1982.3	43.6	0.10	2.31
ICP	92KB1-18	9.7	573	5576	1996.3	39.5	0.10	2.08
ICP	92KB1-4.15	6.5	796	5190	2000.1	78.8	0.10	4.14
ICP	92KB1-13	13.0	452	5880	2067.8	72.1	0.11	3.67

† Format is sample-grain number.spot; ‘c’ indicates core and ‘r’ indicates rim.
‡ ^{204}Pb-corrected values.

Table 2. Summary of Sm/Nd ages from the Dabie–Sulu areas.

Location	Rock	Minerals	Reference	Age	± 2 sigma
2 point isochrons					
Sulu, Rizhao	eclogite	g-c	[69], recalculated	211	19
Dabie, Bixiling	eclogite	g-W	[26]	213	3
Dabie, NOU	eclogite	g-c	[78]	213.6	5.1
Dabie, Bixiling	eclogite	g-c	[26]	218	4
Dabie, NOU	eclogite	g-W	[78]	219.3	6.1
Sulu, Rizhao	eclogite	g-c	[69], recalculated	220.9	5.9
Dabie, Shuanghe	gneiss	g-ky	[23]	229	4
Dabie, Shuanghe	gneiss	g-W	[23]	238	4
Dabie, Shuanghe	eclogite	g-W	[24]	241.9	3.2
Dabie, Wumiao	eclogite	g-W	[79]	246	6
Note that the uncertainties on the 2-point isochrons reflect only measurement error.					
3-or-more point isochrons					
Dabie, Bixiling	eclogite	g-c-W	[26]	210	9
Dabie, Bixiling	g peridotite	g-c-W	[26]	210	7
Dabie, Bixiling	eclogite	g-c-W	[26]	211	4
Dabie, Bixiling	eclogite	g-c-W	[26]	214	7
Dabie, Bixiling	eclogite	g-c-W	[26]	215	5
Dabie, NOU	eclogite	g-c-rut-W	[80]	219	11
Dabie, Shima	eclogite	g-g-c	[69], recalculated	220.6	5.3
Dabie, Maowu	eclogite	g-c-W	[81]	221	5
Dabie, Bixiling	eclogite	g-g-g-g-g-g-g	[26]	225	7
Dabie, Shuanghe	eclogite	g-c-rut	[24]	226.3	3.2
Dabie, Shuanghe	gneiss	g-phe-phe	[24]	226.5	2.3
Sulu, Qinglongshan	eclogite	g-c-phe-WR	[22]	226.5	9.7
Dabie, Gaobayan	gneiss	g-g-g-W	[69], recalculated	228	15
Sulu, Zhubian	eclogite	g-phe-WR	[22]	228.5	8.6
Dabie, NOU	eclogite	g-c-W	[80]	229	13
Dabie, Maowu	g websterite	g-g-c-c-WR	[81]	231	16
Dabie, Maowu	g websterite	g-c-WR-WR	[81]	236	19
Dabie, Raobazhai	g pyroxenite	g-c-W	[69], recalculated	243.5	8.9

“c”, clinopyroxene; “g”, garnet, “phengite”, phengite; “rut”, rutile; “W”, whole rock.

Table 3. Summary of Triassic–Jurassic U/Pb zircon and Th/Pb monazite ages from Dabie and Sulu.

Location	Minerals	Rock	Reference	Age	± 2 sigma
Dabie, Maowu	mnz	clinopyroxenite	[82]	209	2
Dabie, Shuanghe	mnz cores	jadeite quartzite	[82]	223	1
Dabie, Shuanghe	mnz rims	jadeite quartzite	[82]	209	3
Sulu, S of Weihai	zrc	orthogneiss	99SMC6	202.4	2.7
Sulu, CCSD core	zrc	gneiss	[31]	210.8	8.1
Hong'an	zrc	eclogite	[32]	213	5
Dabie, Wumiao	zrc	eclogite	[68]	214.2	9.6
Sulu, CCSD core	zrc	gneiss	[31]	215.1	3.2
Sulu, Yangkou	zrc	orthogneiss	94YK46	216.3	2.4
Sulu, Donghai	zrc	eclogite	[68]	217.1	8.7
Dabie, Jurassic sediments	mnz rims	eclogite	[68]	218.4	2.5
Dabie, SE of Banzhu	zrc	eclogite	[68]	218.5	1.8
Dabie, Wumiao	zrc	gneiss	[83]	218.5	1.7
Sulu, Suoloushu	zrc	orthogneiss	DPC2	218.7	2.2
Dabie, Jurassic sediments	mnz rims	gneiss cobble	[65]	221	1.7
Sulu, Rongcheng	zrc	post-UHP pluton	[28]	219.7	2.1
Sulu, Rongcheng	zrc	post-UHP pluton	[28]	222.1	1.6
Sulu, Rongcheng	zrc	post-UHP pluton	[28]	225.3	1.9
Dabie, Huangzhen	zrc	eclogite	[25]	222	4
Dabie, Wumiao	zrc	gneiss	[30]	222.6	5
Sulu, CCSD core	zrc	paragneiss	[31]	224	2.3
Sulu, Weihai	zrc	orthogneiss	94WHB05	224.5	4.9
Dabie, Maowu	zrc	eclogite	[83]	225.3	4.5
Dabie, E of Yingshan	zrc	gneiss	[42]	225.3	4.8
Dabie, Jurassic sediments	zrc	gneiss cobble	[65]	226	2
Sulu, Donghai	zrc	orthogneiss	95HZ14A	226	4.6
Sulu, Weihai	zrc	peridotite	[70]	226.4	3.6
Sulu, CCSD core	zrc	paragneiss	[31]	227.5	5.4
Sulu, CCSD core	zrc	paragneiss	[31]	227.6	5.1
Sulu, Rongcheng	zrc	orthogneiss	94MY08A	227.8	2.7
Sulu, CCSD core	zrc	gneiss	[31]	228.6	2.1
Dabie, Maowu	zrc	eclogite	[82]	229.6	2.6
Sulu, Weihai	zrc	eclogite	[70]	232	56
Dabie, Shuanghe	zrc	gneiss	[23]	233	21
Dabie, Shima, DS107	zrc	gneiss	[42]	236	3
Dabie, Huangzhen	zrc	gneiss	[25]	236.1	8.4
Dabie, Shima	zrc	?	[84]	236.2	2.4
Dabie, Shuanghe	zrc	?	[84]	236.4	1.2
Dabie, Shuanghe	zrc	jadeite quartzite	[82]	238	3
Dabie, Huangzhen	zrc	eclogite	[25]	243	4
Dabie, Jurassic sediments	zrc	gneiss cobble	[65]	244	5

References Cited

71 F. Corfu, J.M. Hanchar, P.W.O. Hoskin and P.D. Kinny, Atlas of zircon textures, Reviews in Mineralogy and Geochemistry 53, 469-500, 2003.

72 J.S. Stacey and J.D. Kramers, Approximation of terrestrial lead isotope evolution by a two-stage model, Earth and Planetary Science Letters 26, 207-221, 1975.

73 X. Quidelleur, M. Grove, O. Lovera, T.M. Harrison, A. Yin and F.J. Ryerson, The thermal evolution of the Renbu–Zedong thrust, southeastern Tibet, Journal of Geophysical Research 102, 2659-2679, 1996.

74 C.F. Miller, R.D.J. Hatcher, J.C. Ayers, C.D. Coath and T.M. Harrison, Age and zircon inheritance of eastern Blue Ridge plutons, southwestern North Carolina and northeastern Georgia, with implications for magma history and evolution of the southern Appalachian orogen, American Journal of Science 300, 142–172, 2000.

75 J.B. Paces and J.D.J. Miller, Precise U-Pb ages of Duluth Complex and related mafic intrusions, northeastern Minnesota: Geochronological insights to physical, petrogenetic, paleomagnetic, and tectonomagmatic processes associated with the 1.1 Ga Midcontinent Rift System, Journal of Geophysical Research 98, 13997–14013, 1993.

76 K.R. Ludwig, Isoplot/EX, rev. 2.49. A Geochronological Toolkit for Microsoft Excel, Berkeley Geochronology Center Special Publication 1a, 2001.

77 J.N. Aleinikoff, Deciphering igneous and metamorphic events in high grade rocks of the Wilmington Complex, Delaware: Morphology, CL and BSE zoning, and SHRIMP U-Pb geochronology of zircon and monazite, Geological Society of America Bulletin, 2005.

78 Y.-C. Liu, S.-G. Li, S.-T. Xu, B.-m. Jahn, Y.-F. Zheng, Z.-Q. Zhang, L.-L. Jiang, G.-B. Chen and W.-P. Wu, Sm-Nd dating of eclogites from North Dabie and its constraints on the timing of granulite-facies retrogression, Geochimica 30, 79-87, 2001.

79 A.I. Okay, A.M.C. Sengör and M. Satir, Tectonics of an ultrahigh-pressure metamorphic terrane: the Dabie Shan/Tongbai Shan orogen, China, Tectonics 12, 1320–1334, 1993.

80 Z. Xie, Y.-F. Zheng, B.-m. Jahn, M. Ballevre, J. Chen, P. Gautier, T. Gao, B. Gong and J. Zhou, Sm–Nd and Rb–Sr dating of pyroxene–garnetite from North Dabie in east-central China: problem of isotope disequilibrium due to retrograde metamorphism, Chemical Geology 206, 137-158, 2004.

81 B.-m. Jahn, Q. Fan, J.-J. Yang and O. Henin, Petrogenesis of the Maowu pyroxenite–eclogite body from the UHP metamorphic terrane of Dabieshan: chemical and isotopic constraints, Lithos 70, 243-267, 2003.

82 J.C. Ayers, S. Dunkle, S. Gao and C. Miller, Constraints on timing of peak and retrograde metamorphism in the Dabie Shan ultrahigh-pressure metamorphic belt, east-central China, from U-Th-Pb dating of zircon and monazite, Chemical Geology 186, 315–331, 2002.

83 D.B. Rowley, F. Xue, R.D. Tucker, Z.X. Peng, J. Baker and A. Davis, Ages of ultrahigh pressure metamorphism and protolith orthogneisses from the eastern Dabie Shan: U/Pb zircon geochronology, Earth and Planetary Science Letters 151, 191–203, 1997.

84 S. Li, Isotopic geochronology, in: Ultrahigh- Pressure Metamorphic Rocks in the Dabieshan–Sulu Region of China. Petrology and Structural Geology, C. Bolin, ed., pp. 90–105, Kluwer Academic Publishing, Dordrecht, The Netherlands, 1996.